A pigment-deficient mosquito line with fluorescent salivary glands enables *in vivo* imaging of individual *Plasmodium* sporozoites

Dennis Klug[1,#], Katharina Arnold[1,2], Eric Marois[1] and Stéphanie A. Blandin[1]

[1]Université de Strasbourg, CNRS UPR9022, INSERM U1257, Institut de Biologie Moléculaire et Cellulaire, 67000 Strasbourg, France

[2]Current address: German Cancer Research Institute (DKFZ), 69120 Heidelberg, Germany

to whom correspondence should be addressed:
dklug@unistra.fr

Abstract

Plasmodium parasites are the causative agent of malaria, a major health burden in sub-Saharan Africa. A key step in the transmission process of *Plasmodium* is the colonization of the salivary glands of the female *Anopheles* mosquito by the parasite sporozoite stage. How sporozoites recognize and invade the salivary glands is still poorly understood. Here we generated salivary gland reporter lines in the African malaria mosquito *Anopheles coluzzii* using salivary gland-specific promoters of the genes encoding anopheline antiplatelet protein (AAPP), the triple functional domain protein (TRIO) and saglin (SAG). The observed expression pattern of the DsRed and roGFP2 fluorescent reporters revealed lobe-specific activity of these promoters within the salivary glands, restricted either to the distal lobes or the middle lobe. We characterized four mosquito lines (AAPP-DsRed, AAPP-roGFP2, TRIO-DsRed and SAG-EGFP) in terms of localization, expression strength and onset of expression, as well as potential influences of the expressed fluorescent reporters on the infection with *Plasmodium berghei* and salivary gland morphology. Furthermore, using crosses with a pigmentation deficient *yellow(-)* mosquito line, we demonstrate that our salivary gland reporter lines represent a valuable tool to study the process of salivary gland colonization by *Plasmodium* parasites in live mosquitoes.

Introduction

Vector borne diseases have been a major health burden in the history of mankind. An efficient way to counteract diseases transmitted by blood sucking arthropods is to prevent transmission itself by reducing the number of vectors in the environment or by preventing vectors from biting humans in risk areas. As a consequence of malaria control interventions, approximately 663 million clinical malaria cases could be averted between 2000 and 2015. The most effective measure turned out to be the use of insecticide treated bet nets which prevented an estimated 68% of cases (Bhatt *et al.*, 2015). Still, preventive measures are counteracted by the very effective transmission of vector borne pathogens, which hampers eradication approaches. This is especially true for the causative agent of malaria, a protist named *Plasmodium*, which evolved highly specific adaptations to ensure efficient transmission between mosquitoes and human.

After infection of the mosquito midgut through the uptake of a blood meal from an infected host, *Plasmodium* parasites form a cyst, called oocyst, below the basal lamina of the midgut epithelium where they undergo multiple rounds of DNA replication. Rapid cell division, called schizogony, then follows, leading to the generation of several thousand of sporozoites per oocyst. These cells are released from the cysts and travel from the midgut to the salivary glands and, after being deposited in the skin during a blood meal, traverse the dermis, enter blood capillaries and reach the human liver. The sporozoites' distinctive cell polarization and crescent shape, in combination with high motility, allows them to „drill" through tissues. In addition, sporozoites are highly deformable enabling passing through densely packed environments. An important feature of sporozoites is their long survival time, up to several weeks, in mosquito tissues (Mayne, 1922).

While it is believed that the invasion process of the salivary glands by sporozoites that have egressed from oocysts is rapid (~1-10 minutes), *in vivo* data supporting this assumption is lacking (Douglas *et al.*, 2015). Still, the time a sporozoite needs to reach and successfully invade the glands is an important parameter, because at this timepoint, a mosquito is considered infective to humans. Moreover, the very quick invasion of the salivary glands suggests that sporozoites have specific receptors that recognize ligands exposed on the gland surface. Up to date only two mosquito proteins, saglin and circumsporozoite protein (CSP) binding protein (CSPBP), have been described to support salivary gland invasion of sporozoites (Ghosh and Jacobs-Lorena, 2009; Wang *et al.*, 2013). Knockdown experiments of both proteins have shown that sporozoite numbers in the salivary glands are reduced

compared to controls, indicating a lower invasion rate. However, overexpression of saglin in the distal lobes of *Anopheles stephensi* did not lead to an increase in the number of salivary gland resident sporozoites, and immunofluorescence-staining using anti-saglin antibodies indicated that this protein is expressed in the middle lobe of each salivary gland (O'Brochta *et al.*, 2019). This observation is puzzling since sporozoites strongly prefer to invade the distal lobes, with sporozoite invasion of the smaller middle lobe being less prominent or even completely absent (Wells and Andrew, 2019). Thus, the relation between saglin and sporozoites may be more complex than a simple ligand-receptor interaction. Microscopic studies of infected glands revealed that sporozoites form large accumulations in organized „stacks" inside cavities of acinar cells. The astonishing degree of order of these structures raises the question whether sporozoites can recognize each other. Alternatively, specifically preferred invasion sites may lead to accumulations at these entry points. However, since receptor-ligand interactions between sporozoites and acinar cells are still undefined, no specific entry site has been identified thus far.

Proteins secreted in the saliva of blood-sucking arthropods have been a long-term focus of interest. Saliva proteins often possess vasodilating, anti-coagulating and anti-inflammatory properties which counteract host responses and enable efficient blood feeding (Ribeiro and Francischetti, 2003). One protein specifically found in *Anopheles gambiae* saliva is TRIO (triple functional domain protein) that shares low homology to *Drosophila melanogaster* TRIO (Francischetti *et al.*, 2002, Arcà *et al.*, 2005, Dragovic *et al.*, 2018). Interestingly TRIO expression increases in the presence of *P. berghei* sporozoites (Dragovic *et al.*, 2018). The anopheline antiplatelet protein (AAPP) has anti-thrombotic functions and prevents collagen-induced platelet aggregation (Yoshida *et al.*, 2008; Hayashi *et al.*, 2012). Consistently, transgenic co-expression of an AAPP-specific single chain antibody blocking AAPP function negatively affects blood feeding *in vivo* (Islam *et al.*, 2019). The region upstream of the *aapp* gene was the first promoter used to drive salivary gland-specific transgenes in the Asian malaria mosquito *Anopheles stephensi* (Yoshida and Watanabe, 2006). Here we compare the promoter activities of the regions upstream of the *aapp*, *trio* and *saglin* genes in African *Anopheles coluzzii* mosquitoes and we test potential applications of the generated reporter lines to investigate sporozoite migration.

99 # Results

100

101 **Generation of transgenic mosquito lines with salivary gland-specific reporter expression**
102 **and low pigmentation**

103 To generate salivary gland reporter lines, the 5' upstream sequences of *saglin* (AGAP000610),
104 *aapp* (AGAP009974) and *trio* (AGAP001374) were used to drive the expression of DsRed
105 and hGrx1-roGFP2 from transgenic constructs integrated in the X1 docking line (**Fig. 1A, Fig.**
106 **S1**) (Volohonsky *et al.*, 2015). The fluorescence reporter hGrx1-roGFP2 was chosen because
107 it bears the advantages of EGFP and enables the measurement of the oxidation level of the
108 intracellular glutathione pool by ratiometric quantification (Gutscher *et al.*, 2008). We used
109 the *aapp* promoter sequence from *Anopheles coluzzii* orthologous to the one used to drive
110 salivary gland-specific transgene expression in *Anopheles stephensi* (Yoshida and Watanabe,
111 2006). For both *saglin* and *trio*, we defined putative promoter regions according to the
112 genomic context. In addition, as the selected *saglin* promoter region was very short (220bp,
113 **Fig. S2**), we also used CRISPR/Cas9 to integrate a fluorescence cassette encoding EGFP into
114 the endogenous *saglin* locus, replacing the coding sequence, to study *saglin* promoter activity
115 in its native genomic context. For this, site directed knock-in mutagenesis was performed by
116 injecting a plasmid encoding three guide RNAs targeting *saglin* and carrying a repair template
117 marked with *3xP3*-EGFP into mosquito eggs from a line with germline-specific expression of
118 Cas9 (*vasa-Cas9*), generating a *sag(-)KI* line (**Fig. 1B, S3A**). To place the *EGFP* gene
119 directly under control of the *saglin* promoter, the *3xP3* promoter used to selected transgenic
120 mosquito larvae was flanked by lox sites to enable its excision by Cre recombination (**Fig.**
121 **S3E**, Material & Methods). Similarly, we generated a knockin (KI) into the *yellow* gene that
122 encodes a protein required for the synthesis of black pigments in insects (Hunt and Bridges,
123 1916; Wittkopp, True and Carroll, 2002). For this, we used a plasmid with guide RNAs
124 specific for *yellow* and corresponding homology arms flanking a fluorescence cassette
125 expressing EGFP surrounded by lox sites (**Fig. S3B**). Through crossing of salivary gland
126 reporter lines with low pigmented *yellow(-)KI* mosquitoes, we aimed to improve the
127 fluorescence signal of the expressed reporter and extend the range of applications, e.g. for *in*
128 *vivo* imaging. Genotyping by PCR confirmed the successful generation of the salivary gland
129 reporter lines *aapp-DsRed*, *aapp-hGrx1-roGFP2*, *trio-DsRed* and *sag-DsRed* (**Fig S1**) as well
130 as the mosquito lines *sag(-)KI* and *yellow(-)KI* (**Fig S3C,D**). Loss of the *3xP3* promoter in
131 *sag(-)EX* mosquitoes (mosquitoes lacking the *3xP3* promoter after *Cre* mediated excision)

132 was confirmed by PCR in the progeny of a cross between the *sag(-)KI* line and a mosquito
133 line expressing *Cre* recombinase in the germline (**Fig. S3E**) (Volohonsky *et al.*, 2015).
134
135 **Lobe-specific transcriptional activation by *sag*, *aapp* and *trio* promoter sequences**
136 Dissection of female salivary glands revealed a highly specific expression pattern of DsRed,
137 EGFP and hGrx1-roGFP2 driven by *sag, aapp* and *trio* promoter sequences inside salivary
138 glands (**Fig. 1C**). While no fluorescence was observed for DsRed driven by the cloned 5'
139 upstream sequence of the *saglin* gene in dissected salivary glands (**Fig. S3A**), promoter
140 activity was detected in the line where *EGFP* replaced the *saglin* gene (**Fig. 1C**), indicating
141 that essential transcriptional elements localize outside of the intergenic sequence between
142 *AGAP000609* and *AGAP000610* (*saglin*) (**Fig. S3B**). Interestingly, fluorescence signals in
143 glands of female *aapp-DsRed*, *aapp-hGrx1-roGFP2* mosquitoes were restricted to the distal
144 lobes, while female *trio-DsRed* and *sag(-)EX* mosquitoes displayed fluorescence exclusively
145 in the middle lobe (**Fig. 1C**). This difference became especially evident when crossing *aapp-*
146 *hGrx1-roGFP2* mosquitoes with *trio-DsRed* mosquitoes giving rise to a trans-heterozygous
147 offspring displaying hGrx1-roGFP2 expression in distal lobes combined with DsRed
148 expression in the middle lobe (**Fig. 1C**). Similarly, when crossing *aapp* and *trio* DsRed
149 reporter lines, the entire salivary gland was red fluorescent in the F1 progeny (**Fig. 1C**).
150 Expression of *trio-DsRed* and *aapp-DsRed* was so strong that the respective parts of the
151 salivary gland appeared pink colored even in brightfield microscopy (**Fig. 1C**). Of note,
152 fluorescent reporter expression in the salivary glands of *aapp-DsRed*, *aapp-hGrx1-roGFP2*
153 and *trio-DsRed* mosquito colonies was restricted to females while no fluorescence signal
154 could be observed in this organ in males (**Fig. S4A**). Imaging of *aapp-DsRedP*, *aapp-hGrx1-*
155 *roGFP2* and *trio-DsRed* pupae during development revealed no distinct fluorescence signal in
156 the head part where the salivary glands are located (**Fig. S4B**). Still, DsRed expression was
157 visible in the salivary glands of *aapp-DsRed* females that had been dissected directly after
158 emergence (**Fig. 2A**), indicating that the *aapp* promoter is already active in pharate adults. In
159 contrast, no DsRed expression was observed in the glands of freshly hatched *trio-DsRed*
160 females (**Fig. 2A**). To evaluate the expression profile over time we performed a time-course
161 experiment by dissecting and imaging salivary glands of *trio-DsRed* and *aapp-DsRed* females
162 every day. DsRed expression guided by *aapp* and *trio* promoters increases steadily until day 5
163 after hatching (**Fig. 2B**). The strongest increase in fluorescence in *aapp-DsRed* females was
164 observed from day three to four, and from day four to five in *trio-DsRed* females (**Fig. 2B**).
165 The increase in DsRed in the salivary glands of *aapp-DsRed* and *trio-DsRed* females could

166 also be followed in transmitted light based on the pink coloration of the distal lobes (**Fig.**
167 **S4C**). In *Anopheles stephensi,* AAPP expression was shown by qRT-PCR to be upregulated
168 upon blood feeding (Yoshida and Watanabe, 2006). We followed DsRed fluorescence levels
169 in the salivary glands of *aapp-DsRed* and *trio-DsRed* sibling mosquitoes that were fed on
170 blood or kept on sugar (**Fig. 2C**). Our results confirm that the *aapp* promoter is induced upon
171 ingestion of a blood meal while there was no difference between blood-fed and sugar-fed in
172 females expressing the *trio-DsRed* transgene.
173
174 **Subcellular localization of fluorescent reporters and impact on salivary gland**
175 **morphology**
176 During first microscopic examinations using low magnification, different intracellular
177 localizations of the fluorescent proteins DsRed, EGFP and hGrx1-roGFP2 were observed (**Fig.**
178 **1C**), which was confirmed by confocal microscopy. DsRed expressed in the salivary glands
179 of *aapp-DsRed* and *trio-DsRed* mosquitoes appeared spotty and localized in vesicles within
180 the cytoplasm of the acinar cells, while hGrx1-roGFP2 and EGFP expressed in the glands of
181 *aapp-hGrx1-roGFP2* and *sag(-)KI* mosquitoes displayed a cytoplasmic localization (**Fig. 3A**).
182 Due to the anatomy of the secretory cells, which form an inward cavity into which saliva is
183 secreted, the DsRed-positive vesicles localize mainly at the outer rim of the salivary gland. In
184 contrast, localization of hGrx1-roGFP2 and EGFP was homogenous in the cytoplasm and
185 appeared to be also nuclear (**Fig. 3A**). We also observed morphological alterations. While
186 salivary glands of *aapp-DsRed*, *trio-DsRed* and *sag(-)KI* females were indistinguishable from
187 wild type (*G3*), the apex of the distal lobes in *aapp-hGrx1-roGFP2* expressing salivary glands
188 appeared shrunken and we detected a strangulation between the apex and the remainder of the
189 lobe (**Fig. 3B,C**). Acinar cells in the apex of the lobes that displayed the highest expression
190 levels of hGrx1-roGFP2, appeared thinned and atrophied, and presented an inflation of the
191 salivary duct in the apex region (**Fig. 3A**).
192
193 **Natural variation of DsRed expression in *trio-DsRed* mosquitoes**
194 During the generation of the salivary gland reporter lines and their subsequent outcrossing we
195 observed that most L1 mosquito larvae carrying the *trio-DsRed* transgene displayed DsRed
196 expression in the eyes (**Fig. S5A**), which was absent in the two other reporter lines *aapp-*
197 *DsRed* and *aapp-hGrx1-roGFP2*. Interestingly, a few L4 stage larvae of the *trio-DsRed* line
198 even displayed strong ubiquitous DsRed expression (**Fig. S5A**). At the pupal stage, DsRed
199 expression was detected in the ocellus, an eye spot close to the main compound eye, the

antennae and/or throughout the body. The observed expression patterns were highly variable and ranged from completely non-fluorescent pupae to pupae expressing DsRed in all three tissues (**Fig. S4B, S6A**). In adult mosquitoes, DsRed expression was less distinct compared to pupae although complete body fluorescence was occasionally observed in both males and females, with the strongest expression of DsRed in the salivary glands of females and the palps and antennae of males (**Fig. S5B**). Dissections of adult mosquitoes displaying whole body fluorescence at the pupal stage revealed strong and sex-independent DsRed signals in Malphigian tubules, an insect organ that performs functions similar to the vertebrate kidney (**Fig. S5C**). Of note, fluorescence in tubules strictly correlated to the high pupal fluorescence phenotype and was never observed in mosquitoes hatched from low fluorescent pupae (**Fig. S5D**). We next investigated sex-specificity of each fluorescence pattern at the pupal stage and inheritance of the high and low fluorescent *trio-DsRed* transgene. Non-fluorescent pupae were always females, while fluorescent antennae were observed exclusively in male pupae (**Fig. S6B**). In contrast, the presence of a fluorescent ocellus or body fluorescence was sex-independent (**Fig. S6B**). Quantification of the observed expression pattern revealed that a fluorescent ocellus, either alone or in combination with body fluorescence, was most frequently observed (**Fig. S6C**). The ratio of pupae that displayed body fluorescence to those that did not was close to 50% (**Fig S6C**). To follow the inheritance pattern of high and low body fluorescence, pupae were separated according to their fluorescence phenotype and intercrossed. Quantification of pupal DsRed expression in the F1 generation revealed a strong enrichment for whole body fluorescence (~80%) if high pupal body fluorescence was selected in the previous generation. In contrast, no pupae with high body fluorescence were observed in the offspring of mosquitoes hatched from low fluorescent pupae (**Fig. S6D**). This result indicates a form of Mendelian inheritance, with the locus conferring high body fluorescence being dominant over that conferring low body fluorescence. To investigate this further, virgin female pupae of the F1 generation displaying high pupal DsRed expression were crossed with wild type males. Ten single female families were created which were all screened for pupal body fluorescence. All families except family 8 displayed a 1:1 distribution for high and low pupal body fluorescence (**Fig. S6E**). Family 8 displayed exclusively high pupal body fluorescence, indicating that the founder female was homozygous for the locus conferring high body fluorescence, while all other females were heterozygous for the „low“ and the „high“ *trio-DsRed* loci. Notably, we detected high DsRed signals in the salivary glands of all adult females in families 5, 6, 7, 8 and 10 (other families were not investigated), regardless of whether individuals hatched from pupae displaying high or low body fluorescence.

234 Genotyping of females homozygous for low *trio-DsRed* or heterozygous for WT/high *trio-*
235 *DsRed* revealed integration of the transgene into the X1 locus as a single copy (**Fig. S7**).
236
237 **Impact of reporter expression on infection with *Plasmodium berghei***
238 To test if the expression of a fluorescent reporter in the salivary glands alters parasite
239 development in the mosquito, we infected the three reporter lines *trio-DsRed*, *aapp-DsRed*
240 and *aapp-hGrx1-roGFP2* as well as the parental line *G3* with the rodent malaria parasite
241 *Plasmodium berghei* line Δp230p-GFP that constitutively expresses EGFP at high levels in all
242 developmental stages (Manzoni *et al.*, 2015). Parasite counts observed in reporter lines varied
243 from 118 to 142 oocysts and were not significantly different from the control (121 oocysts)
244 (**Fig. 4A**). The average number of salivary gland sporozoites at day 17-18 after infection was
245 8.200 to 17.400 sporozoites per mosquito in salivary gland reporter lines vs 9.600 in *G3*
246 controls (**Fig. 4B**). An average of 10.000 sporozoites is what is usually observed in our
247 laboratory, while numbers can fluctuate from 5.000 to more than 20.000 sporozoites per
248 mosquito even in non-transgenic lines, indicating no significant difference between the *G3*
249 control and reporter lines. To normalize the counts of salivary gland sporozoites relative to
250 differences in oocyst numbers, we calculated the number of sporozoites that had successfully
251 invaded the salivary glands per oocyst. Again, no significant difference was detected between
252 reporter lines (86-146 sporozoites per oocyst) and *G3* control (133) mosquitoes (**Fig. 4C**).
253 These results indicate that fluorescence expression in the salivary glands does not affect
254 parasite development in mosquitoes or salivary gland infection with sporozoites.
255
256 **Salivary gland reporter lines as a tool to investigate sporozoite biology / invasion of the**
257 **salivary glands**
258 We next investigated whether our highly fluorescent salivary gland reporter lines could
259 facilitate *in vivo* imaging of *Plasmodium* development through the cuticle of a living
260 mosquito using the same *P. berghei* line *Δp230p-GFP* (**Fig. 5A**). This line is bright enough to
261 make parasites visible through the mosquito cuticle, allowing pre-sorting of infected
262 mosquitoes based on fluorescence in the mosquito midgut, the salivary glands or in the wing
263 joint, a localization where hemolymph sporozoites tend to accumulate. Still, light absorption
264 by the pigmented cuticle and light scattering by chitin generate signal losses reducing image
265 quality and resolution. To reduce light absorption, we crossed *aapp-DsRed* mosquitoes,
266 displaying highly fluorescent salivary glands without altered morphology, with *yellow(-)KI*
267 mosquitoes, a loss-of-function line with low cuticle pigmentation (**Fig. 5A**). Yellow is a

268 protein required for the synthesis of black pigments in insects, its absence renders the cuticle
269 pale and yellowish (Hunt and Bridges, 1916; Wittkopp, True and Carroll, 2002). As expected,
270 *yellow(-)-aapp-DsRed* mosquitoes displayed a low pigmented cuticle in combination with
271 highly fluorescent salivary glands (**Fig. 5B**). The decrease in pigmentation greatly increased
272 the observed GFP signal visible through the cuticle, notably in strongly pigmented areas that
273 appear almost black in WT mosquitoes (**Fig. 5C**). We next imaged mosquitoes infected with
274 *P. berghei Δp230p-GFP* between day 17 and day 20 after infection, when sporozoites have
275 already invaded the salivary glands. In addition, mosquitoes were pre-sorted for GFP
276 fluorescence in the salivary glands (**Fig. S8A**) as well as in the wing joint (not shown) to
277 confirm the presence of sporozoites. While pre-sorting, we observed that the salivary glands
278 in a subset of mosquitoes (less than 1 out of 5) localized very close to the cuticle **(Fig. S8B,C**).
279 To facilitate *in vivo* imaging, we further selected mosquitoes positive for sporozoites and with
280 cuticular localization of at least one salivary gland. Subsequently the legs of selected
281 mosquitoes were removed and mosquitoes were glued on a microscopy slide. To prevent
282 squeezing of mosquitoes, cover slips were prepared with small plasticine feet at each corner,
283 and fixed with nail polish to prevent shifting of the cover against the microscopy slide (**Fig.**
284 **S8D**). Confocal imaging enabled to visualize precisely single sporozoites through the cuticle
285 close to the salivary gland as well as subcellular structures, like the cavities of acinar cells, of
286 the gland itself (**Fig. 6A**). Live imaging revealed that a considerable number of sporozoites
287 persist in tissues close to the gland and sometimes perform active movement (**Fig. 6B,C,**
288 **Movies 1 and 2**). We also observed single sporozoites moving actively through tissues in a
289 back and forth gliding manner (**Fig. 6B**, **Movie 3**) or making contact with the salivary gland
290 although no invasion event could be monitored (**Fig, 6D**).
291

292 ## Discussion

293 Mosquito salivary glands have long interested entomologists, parasitologists, virologists and
294 microbiologists because they are a key organ in the transmission of vector borne diseases.
295 Still, the host-pathogen interactions that allow the specific recognition and colonization of this
296 organ by different pathogens has been understudied, probably in part because of the relative
297 difficulty to access and visualize these processes in comparison to midgut invasion. The
298 reporter lines we generated in this study represent valuable tools to circumvent some of these
299 issues: they allow (1) to easily visualize the glands, even in brightfield or DIC microscopy,

300 (2) to distinguish distal and middle lobes of the salivary glands, and (3) to image single
301 sporozoites in proximity to the salivary glands *in vivo*.
302 We used the promoters of three salivary gland genes, *aapp*, *trio* and *saglin*, to drive
303 fluorescent reporter expression in *A. coluzzii* mosquitoes. The different fluorescence patterns
304 obtained in the salivary glands of these lines show that the proteomes of middle and distal
305 lobes are diverse and most likely contribute different saliva components. In addition, the
306 variable fluorescence intensity in the distal lobes of both *aapp* lines (stronger towards the
307 apex) point towards an even more complex expression pattern along the lobe. Interestingly the
308 *trio* and the *saglin* promoters were only active in the middle lobe, which, for saglin, is
309 coherent with immunofluorescence studies performed in *A. stephensi* (O'Brochta *et al.*, 2019).
310 This observation is puzzling since both proteins have been shown to either influence salivary
311 gland colonization or transmission of *Plasmodium* sporozoites (Ghosh and Jacobs-Lorena,
312 2009; Dragovic *et al.*, 2018) while parasites prefer to invade the distal lobes (Wells and
313 Andrew, 2019) that lack activity of *saglin* and *trio* promoters. A possible explanation is that
314 the site of expression of both proteins is not the site where they interact with parasites.
315 The absence of reporter expression in mosquitoes expressing DsRed controlled by the *saglin*
316 5' upstream sequence is likely due to the shortness of the cloned promoter sequence. The
317 *saglin* gene localizes in the middle of an array of four genes believed to be salivary gland-
318 specific (Francischetti *et al.*, 2002) and separated by short intergenic regions (**Fig. S1**).
319 Regulatory sequences controlling transcription are likely located upstream and/or downstream
320 of this array and might be shared by all four genes.
321 Notably, the reporter lines display different subcellular localizations of hGrx1-roGFP2, EGFP
322 and DsRed. While all expressed fluorescence, proteins lack any targeting signal which could
323 explain a different localization, only hGrx1-roGFP2 and EGFP localized within the cytoplasm.
324 In contrast, DsRed displayed a vesicular pattern in both middle (*trio*) and distal lobes (*aapp*),
325 while a DsRed2 variant driven by the *aapp* promoter in *A. stephensi* mosquitoes was shown to
326 be cytoplasmic (Yoshida and Watanabe, 2006). The difference in localization between DsRed
327 and other fluorescent reporters points to the presence of a cryptic trafficking signal in DsRed
328 recognized by the acinar cells of *A. coluzzii*. Indeed, although we did not investigate their
329 nature, we also observed the presence of vesicles in the salivary glands of wild type
330 mosquitoes with similar distribution and morphology and displaying weak red
331 autofluorescence (**Fig. S3A**). DsRed could potentially be trafficked to this or a similar
332 compartment explaining its unique localization. Differences in salivary gland morphology
333 between *aapp-DsRed* and *aapp-hGrx1-roGFP2* expressing mosquitoes are likely due to the

334 expression of human Glutaredoxin 1 (hGrx1) and not of roGFP2, a protein derived from
335 EGFP with 2 amino acid changes. Indeed, no change in morphology was detected in *sag(-)EX*
336 mosquitoes expressing EGFP alone in the middle lobe. Still, EGFP appeared less expressed in
337 the *sag(-)EX* compared to hGrx1-roGFP2 in *aapp-hGrx1-roGFP2* (**Fig. 1**) and we cannot
338 exclude that the acinar cells of the middle and distal lobes react differently to the expression
339 of the respective reporters or that the cells show different responses to roGFP2 and EGFP.
340 Despite its influence on cell morphology the salivary glands of hGrx1-roGFP2 expressing
341 mosquitoes retained their integrity even with high mosquito age and apoptosis of cells
342 expressing the fluorescent reporter was not observed.
343 We also report a surprisingly large panel of fluorescence patterns in mosquitoes expressing
344 the *trio-DsRed* transgene. The *trio* promoter activated transcription of DsRed in the salivary
345 glands of all females (but not in males), but also in ocelli, antennae and Malpighian tubules as
346 well as whole body in some but not all mosquitoes, independently of their sex and with a
347 strict correlation between strong DsRed expression in pupal body and adult Malpighian
348 tubules. The fact that *trio* expression was reported to be salivary gland-specific (Dragovic *et*
349 *al.*, 2018) suggests that the region we selected upstream of *trio* does not contain all regulatory
350 elements that control its natural expression, or that the genomic context of the X1 locus may
351 influence its expression. Up to date, the number of available promoters able to drive
352 ubiquitous expression of transgenes in *Anopheles* mosquitoes is limited (Adolfi *et al.*, 2018),
353 thus replacing DsRed in a selected highly fluorescent line could provide a new means to
354 ubiquitously express transgenes. By sorting and crossing according to the observed pupal
355 fluorescence phenotype, it was possible to separate alleles conferring high and low pupal
356 body fluorescence, which allowed the production of a colony enriched with the high pupal
357 fluorescence phenotype and a colony showing only low pupal body fluorescence, especially
358 in the ocelli. This observation pointed towards a genetically encoded difference which is
359 inherited in a Mendelian manner rather than a transient (epi)genetic modification. Genotyping
360 confirmed the presence of a single copy of the transgene in the X1 locus in all types of
361 mosquitoes. Since fluorescent ocelli, antennae and whole body expression were only observed
362 in the *trio-DsRed* population, we propose that the different DsRed expression patterns are
363 locus-specific effects caused by interactions between the selected *trio* promoter sequence and
364 regulatory elements within sequences flanking the transgene, or in trans. The transgene
365 integration into the X1 locus may also have occurred with slight alterations that could
366 influence DsRed expression or a subset of mosquitoes may have inherited a second copy of
367 the transgene integrated in a different locus causing different locus-specific expression effects.

368 However, DsRed positive ocelli and antennae were observed in both high and low
369 fluorescence populations, which is most likely explained by a variable DsRed expression
370 from the transgene inserted at X1. While the observed DsRed expression patterns in larvae
371 and pupae are helpful in the laboratory to select transgenic individuals it also urges caution in
372 interpreting results as it clearly shows that transcription is contextual.
373 Intravital imaging has revealed the dynamics of parasite development inside its vertebrate
374 host (Sturm *et al.*, 2006; Wang *et al.*, 2020). While optical windows in mice is a well
375 implemented method (De Niz *et al.*, 2019), *in vivo* imaging through the cuticle of insects is
376 scarcely performed, mostly because it is difficult to achieve good resolution by imaging
377 through the insect cuticle that scatters and absorbs light very efficiently. Recent studies have
378 explored the possibility to circumvent this issue through the application of clearing protocols
379 on infected mosquitoes to improve resolution and enable imaging through whole mosquitoes
380 (de Niz *et al.*, 2019; Mori, Hirai and Mita, 2019). However, while these improvements are
381 remarkable, imaging of cleared specimens only represents snapshots whereas mapping of
382 dynamic processes would be desired. Imaging of tissues *ex vivo* in combination with the use
383 of hemolymph-like media allows the observation of dynamic processes (Klug and
384 Frischknecht, 2017). Still, imaging *ex vivo* samples can only be performed for a limited
385 amount of time and artifacts due to the artificial tissue environment cannot be excluded. A
386 step forward towards intravital imaging was made recently by developing a protocol that
387 combines feeding of dyes relevant for imaging with blood feeding prior to sample preparation
388 (Trisnadi and Barillas-Mury, 2020). Due to the inflation of the mosquito abdomen directly
389 after feeding, cuticle plates open up and create temporary optical windows that can be
390 exploited for microscopy. Still, in this case, mosquitoes were decapitated and tightly flattened
391 between microscopy slide and cover slip, thus allowing for optimal imaging but maintaining
392 *in vivo* conditions only for a limited time. To demonstrate the use of the salivary gland
393 reporter lines for imaging purposes, we crossed *aapp-DsRed* mosquitoes with the low
394 pigmented mosquito line *yellow(-)KI* deficient for black pigment synthesis. In a subset of
395 mosquitoes, salivary glands localized very closely to the cuticle allowing the recognition of
396 subcellular structures. Combining brighter cuticle with cuticular positioning of the salivary
397 glands within the mosquito thorax was instrumental to achieve visualization of single
398 sporozoites through the cuticle and we were able to get an insight into sporozoite behaviour *in*
399 *vivo*. It is generally believed that sporozoites, after they have been released from the oocyst,
400 are passively transported to the salivary glands and engage in active motility only upon
401 contact with acinar cells (Douglas *et al.*, 2015). Our *in vivo* observations indicate that

402 sporozoites can perform active motility even when not in contact with the salivary gland
403 (**Movie 1**, **2 and 3**). Interestingly, a significant number of sporozoites appeared trapped in
404 close proximity to the gland. These sporozoite accumulations are already known from other
405 sites of the mosquito circulatory system (Hillyer, Barreau and Vernick, 2007). Thus
406 sporozoite localization in the salivary gland area, for example through the detection of GFP,
407 does not necessarily represent a measure for successfully invaded sporozoites (**Fig. 6A**).
408 Here we provide a proof of concept of *in vivo* salivary gland imaging, and we hope that the
409 method can be further improved to gain a better insight of the invasion of salivary glands by
410 sporozoites. The injection of fluorescent beads or dyes could be used as vitality measure to
411 monitor the heartbeat of the mosquito while, at the same time, highlighting contact areas with
412 hemolymph and salivary glands. Also we did not exhaust the repertoire of possible genetic
413 modifications to decrease pigmentation of the cuticle. Deletion of the gene*s tan* and *ebony*,
414 two enzymes which regulate the homeostasis of the pigment precursors dopamine and N-ß-
415 alanyldopamine, in combination with the deletion of *yellow* could potentially further decrease
416 cuticle pigmentation (Wittkopp, True and Carroll, 2002; True *et al.*, 2005). Another
417 possibility could be the overexpression of arylalkylamine-*N*-acetyltransferase, an enzyme
418 converting dopamine into the sclerotizing precursor molecule N-acetyldopamine, which was
419 shown to affect pigmentation in different insect species by enhancing the production of
420 colorless components of the cuticle (Osanai-Futahashi *et al.*, 2012). A key improvement for *in*
421 *vivo* imaging would be an increase in the number of mosquitoes displaying ideally positioned
422 salivary glands. Preliminary monitoring experiments showed that the position of the gland
423 does not significantly change over time in adult mosquitoes indicating that positioning occurs
424 during metamorphosis. Should salivary gland positioning be genetically determined, selective
425 breeding may help to improve the ratio of mosquitoes with cuticular salivary glands. Taken
426 together we hope that the transgenic lines developed in this study can contribute to improve *in*
427 *vivo* imaging and salivary gland dissections in *Anopheles* mosquitoes, and enable real-time
428 imaging of *Plasmodium* and other vector borne pathogens.
429

430 ## Materials & methods

431

432 **Animals**

433 Transgenesis was performed in the *Anopheles coluzzii* strain X1 (Volohonsky *et al.*, 2015) or
434 in a strain expressing Cas9 from the X1 locus under control of the *vasa* promoter

435 (transgenesis plasmid: Addgene # 173670) and introgressed into the *Ngousso* genetic
436 background. Wild type *Anopheles coluzzii* strains *Ngousso* and *G3* were used as controls.
437 CD1 mice purchased from Charles River or from our own colonies were used for both
438 mosquito maintenance through blood meals, and for parasite maintenance and mosquito
439 infections. For infections with rodent malaria parasites, we made use of the *Plasmodium*
440 *berghei* line *Δ p230p-GFP* derived from the wild type background *P. berghei ANKA*
441 (Manzoni *et al.*, 2015).
442
443 **Breeding of mosquitoes**
444 *Anopheles coluzzii* mosquitoes were kept in standard conditions (27°C, 75-80% humidity, 12-
445 hr/12-hr light/dark cycle). Larvae were hatched in pans of osmosed water and fed with
446 pulverized fish food (TetraMin, Melle, Germany). Adult mosquitoes were maintained on a
447 10% sucrose solution. To propagate colonies, four to seven day old mosquitoes were blood
448 fed for 10-15 minutes on anesthetized mice and allowed to lay eggs on wet filter paper 2-3
449 days later. For mosquito blood feeding, female CD-1 mice (> 35g) were anesthetized with a
450 mixture of Zoletil (42.5 mg/kg) and Rompun (8.5 mg/kg) in 0.9% NaCl solution.
451
452 **Construction of salivary gland reporter transgenes**
453 The 5'upstream sequences of *saglin* (primers P9 and P10), *aapp* (primers P1 and P2) and *trio*
454 (primers P7 and P8) were amplified from genomic DNA of *G3* mosquitoes isolated with the
455 Blood & Tissue Kit (Qiagen) as shown in **File S1**. DsRed (primers P5 and P6 for *aapp/trio*;
456 P11 and P12 for *saglin*) and hGrx1-roGFP2 (primers P3 and P4) were amplified from the
457 plasmids pJET-DsRed-SV40 and pDSAP_actin-hGrx1-roGFP2 (donated by Raquel Mela-
458 Lopez). Primers are shown in **Table S1**. PCR was performed using Phusion polymerase
459 according to the manufacturer recommendations (ThermoFisher Scientific) and subcloned in
460 the pJET vector using the CloneJET PCR Cloning Kit (ThermoFisher Scientific). The
461 5'upstream sequence of the *saglin* gene was fused to the *DsRed* gene by a Phusion mediated
462 assembly PCR (TerMaat *et al.*, 2009) before cloning into pJET. After sequence verification,
463 assembly blocks were fused into the destination vector pDSAP (Volohonsky et al., 2015,
464 Addgene # 62293) using Goldengate cloning and generating pDSAP-aapp-DsRed, pDSAP-
465 aapp-hGrx1-roGFP2, pDSAP-trio-DsRed and pDSAP-saglin-DsRed.
466
467

468 **Construct cloning for site-directed mutagenesis into *yellow* and *saglin* genes**
469 For the design of guide RNAs (gRNAs), the coding sequence of *saglin* as well as the first
470 exon of the *yellow* gene were manually searched for PAMs (NGG), with N representing any
471 nucleotide. Candidate gRNA sequences were investigated for potential off-target effects using
472 http://www.rgenome.net/cas-designer/ (Cas-OFFinder) (Bae, Park and Kim, 2014). We
473 selected gRNAs starting with a G considering the transcription start from the U6 promoter
474 and differing by ≥3 nucleotides from putative off-target sequences in the *A. coluzzii* genome.
475 For each knockin construct, linkers encoding the protospacer motif of three gRNAs (**Table**
476 **S1**) were generated by annealing two primers ordered from IDT DNA and cloned using *BbsI*
477 into pKSB-sgRNA (Addgene #173671—3) vectors containing the U6 snRNA polymerase III
478 promoter (AGAP013557), the invariable sequence of a standard crRNA-tracerRNA fusion
479 (Jinek et al., 2012), and the RNA polIII TTTTT terminator. The three complete gRNAs
480 blocks were then assembled into a single pKSB-sgRNA destination plasmid by GoldenGate
481 cloning using different but matching *BsaI* overhangs. For the construction of repair templates,
482 regions of homology on the 5' side (*saglin*: primers P29 and P30; *yellow*: primers P19 and
483 P20) and on the 3' side (*saglin*: primers P31 and P32; *yellow*: primers P21 and P22) of the
484 region targeted by the gRNAs were amplified from *Ngousso* genomic DNA and subcloned in
485 the pJET vector, generating plasmids pJET-5'saglin, pJET-5'yellow, pJET-3'saglin and
486 pJET-3'yellow. After sequence validation, all building blocks were fused in the correct order
487 in the destination plasmid pENTR using GoldenGate assembly together with a building block
488 containing either the fluorescence cassette pKSB-Lox3xP3Lox-EGFP or pKSB-Lox3xP3-
489 EGFP-Lox, generating pENTR-Saglin;Lox3xP3Lox-EGFP and pENTR-Yellow;Lox3xP3-
490 EGFP-Lox. Primers are shown in **Table S1**.
491
492 **Transgenesis of *A. coluzzii***
493 All plasmids used for DNA injections were purified using Endofree kits (Qiagen). Freshly
494 laid eggs of the docking line X1 or the *vasa-Cas9* line were injected as described (Fuchs,
495 Nolan and Crisanti, 2013; Pondeville *et al.*, 2014; Volohonsky *et al.*, 2015). For ΦC31-
496 integrase mediated transgensis a mix of three plasmids (pDSAP-aapp-DsRed, pDSAP-aapp-
497 hGrx1-roGFP2 and pDSAP-trio-DsRed) (~160 ng/µL) and the integrase helper plasmid
498 carrying the Vasa2-ΦC31-Integrase gene (Addgene # 62299, ~200 ng/µL) diluted in 0.5x
499 phosphate buffered saline (0.1 mM NaHPO4 buffer, 5 mM KCl, pH 6.8) was injected into
500 approximately 500 embryos. The plasmid pDSAP-saglin-DsRed was injected in the same
501 way but into a different batch of eggs. For site-directed knock-in mediated by Cas9, the

502 plasmid solution (pENTR-Saglin;Lox3xP3Lox-EGFP or pENTR-Yellow;Lox3xP3Lox-
503 EGFP) (~200-300 ng/µL) was diluted in PBS supplemented with 1 µM Scr7 to inhibit non-
504 homologous end joining. Each construct was injected in a separate batch of approximately
505 500 eggs obtained from *vasa-Cas9* females.
506
507 **Salivary gland reporter lines *sag-DsRed, trio-DsRed, aapp-DsRed* and *aapp-hGrx1-***
508 ***roGFP2***
509 Following egg micro-injection, surviving pupae were sorted according to sex, hatched in
510 separate cages (G0 generation) and crossed with ~100 mosquitoes of the other sex from a
511 mosquito line expressing CFP from the X1 docking site that was used as a balancer of the
512 new, non-fluorescent but puromycin resistant transgenic insertions at the same locus. Neonate
513 larvae from this cross were treated with puromycin (0.05 mg/mL). G1 pupae were
514 subsequently sex sorted and crossed with CFP positive mosquitoes to expand the population.
515 Adult puromycin resistant G2 females were sorted according to the observed fluorescence
516 phenotype (DsRed or roGFP2) in their salivary glands, reflecting the expression of the *trio-*
517 *DsRed*, *aapp-DsRed* or *aapp-hGrx1-roGFP2* transgenes and crossed to CFP balancer males.
518 For *sag-DsRed* females, sorting was not necessary, as transgenesis was performed separately
519 by injection of the pDSAP-saglin-DsRed plasmid alone. Puromycin-resistant G3 larvae were
520 raised, intercrossed and the G4 offspring was sorted by COPAS (Marois et al., 2012) for the
521 absence of CFP to select lines homozygous for *sag-DsRed*, *trio-DsRed*, *aapp-DsRed* and
522 *aapp-hGrx1-roGFP2*. Lines were then raised without puromycin treatment. Single females of
523 all generated colonies were genotyped by PCR to monitor correct integration of the transgene
524 into the docking site (**Fig. S1A,B**). Successfully genotyped mosquito colonies were expanded
525 and used to perform experiments.
526
527 ***yellow(-)KI* and *sag(-)KI* lines**
528 Pupae obtained from plasmid injected eggs were sorted according to sex and crossed with 100
529 *Ngousso* wild type partners. G1 neonate larvae were screened for the expression of EGFP
530 using a Nikon SMZ18 fluorescence Stereomicroscope. Selected transgenic larvae were sex
531 sorted at the pupal stage and crossed with an excess of wild type partners. The G2 progenies
532 (from a single positive G1 female for *sag(-)KI* and from 10 positive individuals for *yellow(-*
533 *)KI*) were COPAS sorted to enrich for the integrated transgene and to remove the *vasa-Cas9*
534 transgene (marked with DsRed). The generated *sag(-)KI* colony was kept in equilibrium with
535 the wild type allele, while the *yellow(-)KI* colony was completely homozygotized for the

536 transgene by selecting for mosquitoes with a yellow body color. Homozygous *sag(-)KI*
537 mosquitoes were crossed with the C2S line expressing Cre in the germline (Volohonsky *et al.*,
538 2015) for Cre recombinase-mediated excision of the lox cassette to generate *sag(-)EX*
539 mosquitoes.
540
541 **Genotyping of mosquito lines**
542 Genotyping was performed on genomic DNA extracted from single mosquitoes of *aapp-*
543 *DsRed*, *aapp-hGrx1-roGFP2*, *trio-DsRed*, *sag(-)KI, sag(-)EX* and *yellow(-)KI* colonies.
544 Genotyping PCRs were performed using GoTaq Green Mastermix (Promega) (**Fig. S1B**),
545 Phusion polymerase (ThermoFisher Scientific) or the Phire Tissue Direct PCR Master Mix
546 (ThermoFisher Scientific) (**Fig. S2** and **S7**) according to manufacturer recommendations. See
547 **Table S2** for genotyping primers.
548
549 **Mosquito infection and evaluation of parasite numbers**
550 Parasites were maintained as frozen stocks at -80ºC or by passage between mice. For this,
551 blood was taken by heart puncture from a donor mouse with a parasitaemia of 3-5%, diluted
552 to 2.10^7 parasitized erythrocytes in 100 µL 0.9% NaCl that were injected intravenously into a
553 naïve mouse. Parasitemia was monitored via flow cytometry (Accuri C6, BD biosciences)
554 three days later. Mosquitoes were fed for 10-15 min on anesthetized mice with 2.5 – 3.5%
555 parasitemia. Blood fed females were sorted and kept on 10% sucrose at 21ºC and 50-70%
556 humidity. Midguts and salivary glands were dissected in PBS under a SZM-2 Zoom
557 Trinocular stereomicroscope (Optika). Images were acquired with the Nikon SMZ18
558 Stereomicroscope (without coverslip) or with a Zeiss LSM 780 confocal microscope (sealed
559 coverslip). To count oocysts, midguts were dissected 7-8 days post infection. Fluorescence
560 images of infected midguts were processed using the watershed segmentation plugin (Soille
561 and Vincent, 1990) and oocysts were subsequently counted using the „analyze
562 particles“ function implemented in Fiji (Schindelin *et al.*, 2012). To count salivary gland
563 sporozoites, salivary glands were collected in PBS 17-18 days post infection and ground with
564 a plastic pestle for one minute. The number of sporozoites was measured using a Neubauer
565 hemocytometer under a light microscope (Zeiss).
566
567
568

569 **Fluorescence imaging, fluorescence measurements and image analysis**

570 Samples imaged using the Nikon SMZ18 Stereomicroscope were usually acquired using the
571 respective fluorescence filter to visualize expression of DsRed or roGFP2/EGFP combined
572 with brightfield to visualize the whole specimen. Images were taken using a 63-fold
573 magnification objective (NA 1.4) on a Zeiss LSM 780 confocal microscope (**Fig. 3A**), a
574 Zeiss Axiovert 200 fluorescence microscope **(Fig. S2A**) or using an iPhone 6 for the mounted
575 mosquitoes prepared for microscopy in **Fig. S8D**. All other images as well as images used for
576 fluorescence measurements were acquired with a Nikon SMZ18 Stereomicroscope. For
577 fluorescence quantifications, images were acquired in the DsRed channel and settings were
578 kept the same for all experiments. For each salivary gland, only a single lobe was measured
579 by analyzing a square of 51×51 pixels covering the central part of the fluorescent area to
580 determine the mean fluorescence intensity. The image processing for all experiments was
581 performed with Fiji (Schindelin *et al.*, 2012).

582

583 ***In vivo* imaging**

584 For *in vivo* imaging experiments, infected *yellow(-)-aapp-DsRed* mosquitoes were pre-
585 screened between days 17 - 21 post infection for the presence of hemolymph sporozoites
586 (hinge of the wing, GFP fluorescence) and salivary gland sporozoites (salivary gland, GFP
587 fluorescence) as well as for cuticular positioning of the salivary gland (DsRed signal) (**Fig.**
588 **S8B**). After removing their legs, mosquitoes were glued on a microscopy slide using small
589 amounts of UV-light reactive glue (Bondic Pocket) and covered with a coverslip prepared
590 with plasticine feet at each corner to prevent a squeezing of the sample. Corners of the cover
591 slip were coated with nail polish to prevent sliding. Imaging was performed on a Zeiss LSM
592 780 confocal microscope with GaAsP detector and Metamorph acquisition software.

593

594 **Statistical analysis**

595 Statistical analysis was performed using GraphPad Prism 5.0 (GraphPad, San Diego, CA,
596 USA). Data sets were either tested with a one-way ANOVA or a Student's t test. A value of
597 $p<0.05$ was considered significant.

598

599 **Data availability**

600 All data have been made available within this manuscript. Transgenic mosquito lines as well
601 as plasmids are available upon request.

602

603 **Ethics statement**

604 Experiments were carried out in conformity with the 2010/63/EU directive of the European
605 Parliament on the protection of animals used for scientific purposes. Our animal care facility
606 received agreement #I-67-482-2 from the veterinary services of the département du Bas Rhin
607 (Direction Départementale de la Protection des Populations). The use of animals for this
608 project was authorized by the French ministry of higher education, research and innovation
609 under the number APAFIS#20562- 2019050313288887 v3. The generation and use of
610 transgenic lines (bacteria, mosquitoes, parasite) was authorized by the French ministry of
611 higher education, research and innovation under the number 3243.

612

613 **Funding**

614 This work was supported by the Laboratoire d'Excellence (LabEx) ParaFrap (grant LabEx
615 ParaFrap ANR-11-LABX-0024), by the Equipement d'Excellence (EquipEx) I2MC (grant
616 ANR-11-EQPX-0022), by the ERC Starting Grant Nº260918, and by funding from CNRS,
617 Inserm, and the University of Strasbourg. DK is funded by a DFG postdoctoral fellowship
618 (KL 3251/1-1).

619

620 **Acknowledgements**

621 We thank Amandine Gautier for help with rearing mosquitoes and technical assistance during
622 infections with *P. berghei*, Sarra Manai for help with experiments, Jean-Daniel Fauny for
623 assistance during microscopy and the whole mosquito immune responses (MIR) team for
624 assistance with mosquito breeding and pupae collection.

625

626 Authors contributions

627 DK designed and performed experiments, analyzed data, made figures and wrote the draft.
628 KA cloned constructs, performed initial experiments and analyzed data. EM performed
629 transgenesis of mosquitoes. SB edited the draft and helped with conceptualization of
630 experiments. All authors edited and approved the manuscript for publication.

631

632 Competing interests

633 The authors declare no competing interests.

634 **References**

635 **Adolfi**, A. *et al.* (2018) 'Multi-tissue GAL4-mediated gene expression in all
636 Anopheles gambiae life stages using an endogenous polyubiquitin promoter',
637 *Insect Biochemistry and Molecular Biology*. doi: 10.1016/j.ibmb.2018.03.005.
638
639 **Bae**, S., Park, J. and Kim, J. S. (2014) 'Cas-OFFinder: A fast and versatile
640 algorithm that searches for potential off-target sites of Cas9 RNA-guided
641 endonucleases', *Bioinformatics*. doi: 10.1093/bioinformatics/btu048.
642
643 **Berghammer**, A. J., Klingler, M. and Wimmer, E. A. (1999) 'A universal
644 marker for transgenic insects', *Nature*. doi: 10.1038/46463.
645
646 **Bhatt**, S. *et al.* (2015) 'The effect of malaria control on Plasmodium falciparum
647 in Africa between 2000 and 2015', *Nature*. doi: 10.1038/nature15535.
648
649 **Douglas**, R. G. *et al.* (2015) 'Active migration and passive transport of malaria
650 parasites', *Trends in Parasitology*, pp. 357–362. doi: 10.1016/j.pt.2015.04.010.
651
652 **Dragovic**, S. M. *et al.* (2018) 'Immunization with AgTRIO, a Protein in
653 Anopheles Saliva, Contributes to Protection against Plasmodium Infection in
654 Mice', *Cell Host and Microbe*. doi: 10.1016/j.chom.2018.03.008.
655
656 **Engler**, C. and Marillonnet, S. (2014) 'Golden Gate cloning', *Methods in*
657 *Molecular Biology*. doi: 10.1007/978-1-62703-764-8_9.
658
659 **Francischetti**, I. M. B. *et al.* (2002) 'Toward a catalog for the transcripts and
660 proteins (sialome) from the salivary gland of the malaria vector Anopheles
661 gambiae', *Journal of Experimental Biology*.
662
663 **Fuchs**, S., Nolan, T. and Crisanti, A. (2013) 'Mosquito transgenic technologies
664 to reduce plasmodium transmission', *Methods in Molecular Biology*, 923, pp.
665 601–622. doi: 10.1007/978-1-62703-26-7_41.
666
667 **Ghosh**, A. K. and Jacobs-Lorena, M. (2009) 'Plasmodium sporozoite invasion
668 of the mosquito salivary gland', *Curr Opin Microbiol*, 12. doi:
669 10.1016/j.mib.2009.06.010.
670
671 **Gutscher**, M. *et al.* (2008) 'Real-time imaging of the intracellular glutathione
672 redox potential', *Nature Methods*. doi: 10.1038/nmeth.1212.
673

674 **Hayashi**, H. *et al.* (2012) 'Anopheline anti-platelet protein from a malaria
675 vector mosquito has anti-thrombotic effects in vivo without compromising
676 hemostasis', *Thrombosis Research*. doi: 10.1016/j.thromres.2011.09.015.
677
678 **Hillyer**, J. F., Barreau, C. and Vernick, K. D. (2007) 'Efficiency of salivary
679 gland invasion by malaria sporozoites is controlled by rapid sporozoite
680 destruction in the mosquito haemocoel', *International Journal for Parasitology*.
681 doi: 10.1016/j.ijpara.2006.12.007.
682
683 **Hunt**, T. M. and Bridges, C. B. (1916) *Sex Linked Inheritance in Drosophila*,
684 *Carnegie Institution of Washington*.
685
686 **Islam**, A. *et al.* (2019) 'Anopheline antiplatelet protein from mosquito saliva
687 regulates blood feeding behavior', *Scientific Reports*. doi: 10.1038/s41598-019-
688 39960-2.
689
690 **Klug**, D. and Frischknecht, F. (2017) 'Motility precedes egress of malaria
691 parasites from oocysts', *eLife*, 6.
692
693 **Lee**, J. H. *et al.* (1996) 'Sequential amplification of cloned DNA as tandem
694 multimers using class- IIS restriction enzymes', *Genetic Analysis -*
695 *Biomolecular Engineering*. doi: 10.1016/S1050-3862(96)00164-7.
696
697 **Manzoni**, G. *et al.* (2015) 'A rapid and robust selection procedure for
698 generating drug-selectable marker-free recombinant malaria parasites', *Scientific*
699 *Reports*, 4(1), p. 4760. doi: 10.1038/srep04760.
700
701 **Mayne**, B. (1922) 'How Long Does a Mosquito Retain Malaria Parasites?',
702 *Public Health Reports (1896-1970)*. doi: 10.2307/4576379.
703
704 **Mori**, T., Hirai, M. and Mita, T. (2019) 'See-through observation of malaria
705 parasite behaviors in the mosquito vector', *Scientific Reports*. doi:
706 10.1038/s41598-019-38529-3.
707
708 **Natarajan**, R. *et al.* (2001) 'Fluorescent Plasmodium berghei sporozoites and
709 pre-erythrocytic stages: A new tool to study mosquito and mammalian host
710 interactions with malaria parasites', *Cellular Microbiology*, 3(6), pp. 371–379.
711 doi: 10.1046/j.1462-5822.2001.00117.x.
712
713 **De Niz**, M. *et al.* (2019) '3D imaging of undissected optically cleared
714 Anopheles stephensi mosquitoes infected with Plasmodium parasites', *bioRxiv*.
715 doi: 10.1101/682054.
716

De Niz, M. *et al.* (2019) 'Intravital imaging of host–parasite interactions in skin and adipose tissues', *Cellular Microbiology*. doi: 10.1111/cmi.13023.

O'Brochta, D. A. *et al.* (2019) 'Is Saglin a mosquito salivary gland receptor for Plasmodium falciparum?', *Malaria Journal*. doi: 10.1186/s12936-018-2634-5.

Osanai-Futahashi, M. *et al.* (2012) 'A visible dominant marker for insect transgenesis', *Nature Communications*. doi: 10.1038/ncomms2312.

Pondeville, E. *et al.* (2014) 'Efficient ΦC31 integrase–mediated site-specific germline transformation of Anopheles gambiae', *Nature Protocols*, 9(7), pp. 1698–1712. doi: 10.1038/nprot.2014.117.

Ribeiro, J. M. C. and Francischetti, I. M. B. (2003) 'Role of Arthropod Saliva in Blood Feeding: Sialome and Post-Sialome Perspectives', *Annual Review of Entomology*. doi: 10.1146/annurev.ento.48.060402.102812.

Schindelin, J. *et al.* (2012) 'Fiji: an open-source platform for biological-image analysis', *Nature Methods*, 9(7), pp. 676–682. doi: 10.1038/nmeth.2019.

Soille, P. and Vincent, L. M. (1990) '<title>Determining watersheds in digital pictures via flooding simulations</title>', in *Visual Communications and Image Processing '90: Fifth in a Series*. doi: 10.1117/12.24211.

Sturm, A. *et al.* (2006) 'Manipulation of host hepatocytes by the malaria parasite for delivery into liver sinusoids.', *Science (New York, N.Y.)*, 313(5791), pp. 1287–1290. doi: 10.1126/science.1129720.

TerMaat, J. R. *et al.* (2009) 'Gene synthesis by integrated polymerase chain assembly and PCR amplification using a high-speed thermocycler', *Journal of Microbiological Methods*. doi: 10.1016/j.mimet.2009.09.015.

Trisnadi, N. and Barillas-Mury, C. (2020) ' Live In Vivo Imaging of Plasmodium Invasion of the Mosquito Midgut ', *mSphere*. doi: 10.1128/msphere.00692-20.

True, J. R. *et al.* (2005) 'Drosophila tan encodes a novel hydrolase required in pigmentation and vision.', *PLoS genetics*, 1(5). doi: 10.1371/journal.pgen.0010063.

Volohonsky, G. *et al.* (2015) 'Tools for Anopheles gambiae Transgenesis', *G3 (Bethesda); Genes|Genomes|Genetics*, 5(6), pp. 1151–1163. doi: 10.1534/g3.115.016808.

760 **Wang**, J. *et al.* (2013) 'Anopheles gambiae circumsporozoite protein--binding
761 protein facilitates Plasmodium infection of mosquito salivary glands', *J Infect*
762 *Dis*, 208. doi: 10.1093/infdis/jit284.
763
764 **Wang**, L. T. *et al.* (2020) 'A Potent Anti-Malarial Human Monoclonal Antibody
765 Targets Circumsporozoite Protein Minor Repeats and Neutralizes Sporozoites in
766 the Liver', *Immunity*. doi: 10.1016/j.immuni.2020.08.014.
767
768 **Wells**, M. B. and Andrew, D. J. (2019) 'Anopheles salivary gland architecture
769 shapes plasmodium sporozoite availability for transmission', *mBio*. doi:
770 10.1128/mBio.01238-19.
771
772 **Wittkopp**, P. J., True, J. R. and Carroll, S. B. (2002) 'Reciprocal functions of
773 the Drosophila Yellow and Ebony proteins in the development and evolution of
774 pigment patterns', *Development*.
775
776 **Yoshida**, S. *et al.* (2008) 'Inhibition of collagen-induced platelet aggregation by
777 anopheline antiplatelet protein, a saliva protein from a malaria vector mosquito',
778 *Blood*. doi: 10.1182/blood-2007-06-097824.
779
780 **Yoshida**, S. and Watanabe, H. (2006) 'Robust salivary gland-specific transgene
781 expression in Anopheles stephensi mosquito', *Insect Molecular Biology*. doi:
782 10.1111/j.1365-2583.2006.00645.x.
783

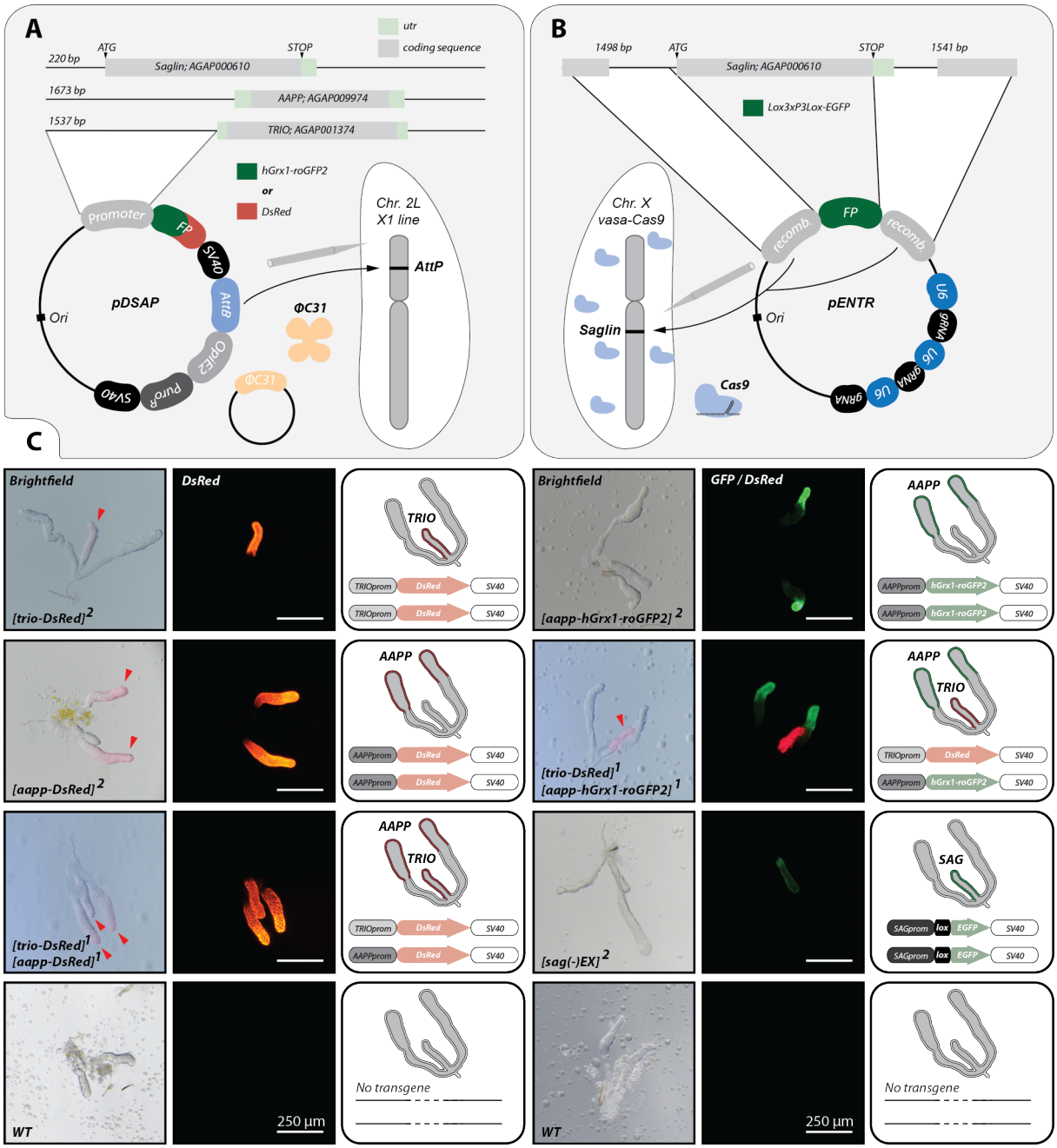

Figure 1. Lobe-specific reporter expression observed in female *aapp-DsRed*, *aapp-hGrx1-roGFP2*, *trio-DsRed* and *sag(-)EX* mosquitoes.

A) ΦC31 integrase-mediated transgene insertion. The *aapp*, *trio* and *saglin* promoter sequences were fused to *DsRed* or *hGrx1-roGFP2* within the pDSAP vector which enables chemical selection of mosquito larvae by puromycin. Transgenes were integrated by ΦC31 integrase-mediated recombination into the X1 line harbouring an *attP* site on chromosome 2L. **B)** Cas9-mediated knockin of a fluorescence cassette in the *saglin* gene (AGAP000610). Upstream and downstream sequences of *saglin* were cloned into the pENTR vector flanking a fluorescence cassette expressing EGFP under the control of the *3xP3* promoter. Three guides targeting *saglin* controlled by *U6* promoters were encoded on the same pENTR vector. Transgenesis was performed in mosquitoes with germline-specific expression of Cas9 (vasa-Cas9). **C)** Fluorescent reporter expression in *trio-DsRed*, *aapp-DsRed*, *aapp-hGrx1-roGFP2* and *sag(-)EX* expressing mosquito females in comparison to wild type (*G3*). Representative

799 images of salivary glands are shown in brightfield beside an image of the same gland in the
800 relevant fluorescence channel. Red arrows in brightfield images highlight the pink parts of
801 *aapp-DsRed* and *trio-DsRed* salivary glands in the absence of fluorescence excitation
802 indicating the high expression of DsRed. The illustration on the right of each panel indicates
803 the genotype of the gland as well as the observed fluorescence pattern. Scale bars: 250 µm.
804

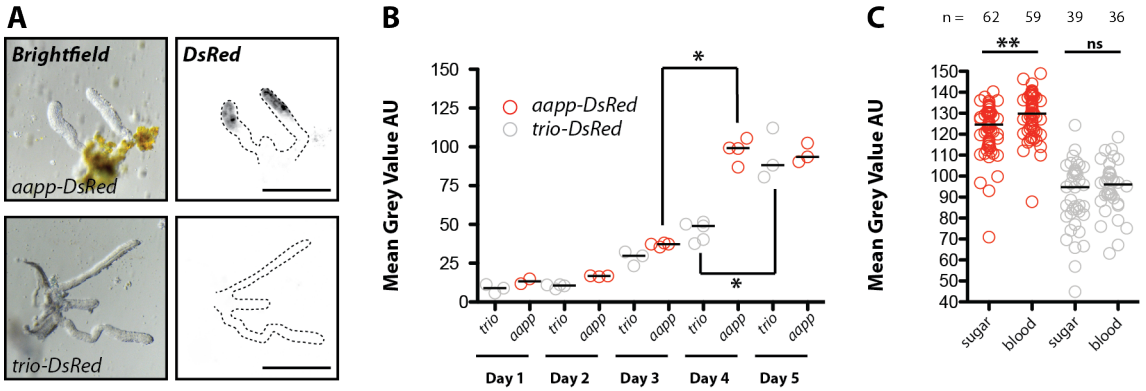

Figure 2. Onset, strength and inducibility by blood feeding of reporter expression in *aapp-DsRed* and *trio-DsRed* mosquitoes.

A) Images of salivary glands dissected directly after mosquitoes emerged. DsRed expression was observed in *aapp-DsRed* but not in *trio-DsRed* expressing salivary glands. Scale bar: 250 µm. **B)** Mean fluorescence intensity measurements of dissected *aapp-DsRed* and *trio-DsRed* salivary glands from day one to day five after hatching. Data were normalized for the highest exposure time. Each dot represents a single gland (2-5 glands / timepoint) and the bars, mean values. *$p<0.05$, Mann Whitney test. **C)** The blood meal inducibility of the *trio* and the *aapp* promoters was assessed by providing sibling females either with a blood meal or sugar solution. Approximately 24h later, salivary glands were dissected, imaged and the mean DsRed fluorescence intensity was quantified. Data pooled from three independent experiments. Same representation and statistical analysis as in (B), **$p=0.0015$.

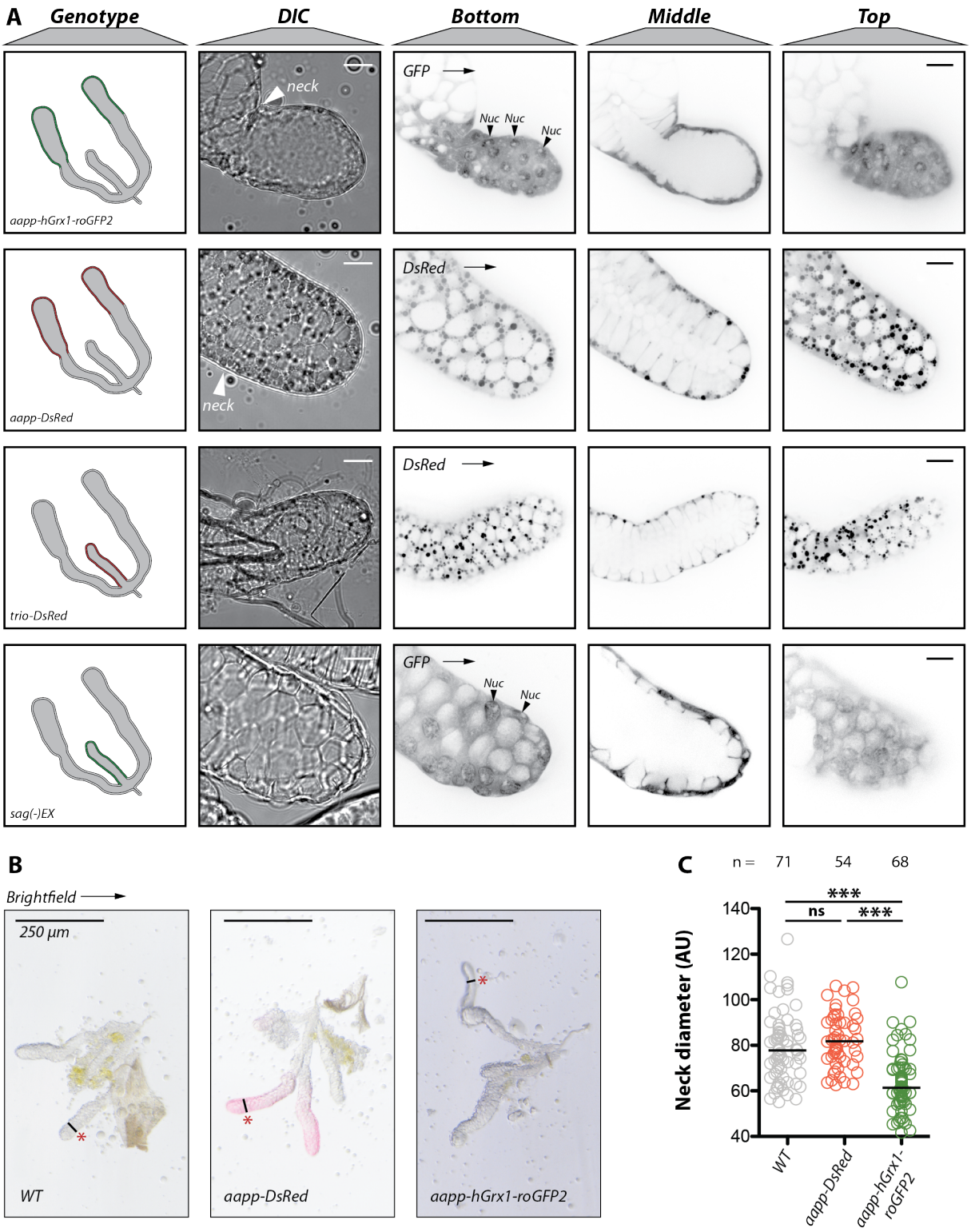

Figure 3. Different subcellular localizations of the expressed DsRed, EGFP and hGrx1-roGFP2 fluorescent reporters.

A) Differential interference contrast (DIC) and confocal fluorescence images of distal (*aapp-DsRed*, *trio-DsRed*) or middle (*trio-DsRed*, *sag(-)EX*) salivary gland lobes. Different z-sections (top, middle and bottom) of the same glands are displayed in the relevant fluorescence channel. The „neck“ regions of the *aapp-DsRed* and *aapp-hGrx1-roGFP2* expressing lobes are indicated by white arrows. Note that DIC and fluorescence images were

taken with a Hamamatsu Orca Flash 4.0 V1 and a Yokogawa CSU X-1 camera, respectively. Images between different channels are therefore not completely matching although depicting the same salivary gland. The illustration on the left depicts the genotype and corresponding expression pattern. Scale bars: 20 µm. **B)** Brightfield images of female wild type (*G3*), *aapp-DsRed* and *aapp-hGrx1-roGFP2* salivary glands. The „neck“ is indicated by a red asterisk and the measured diameter by a black line. Scale bars: 250 µm. **C)** Diameter measurements of the distal lobe neck region of *aapp-DsRed* and *aapp-hGrx1-roGFP2* in comparison to wild type (*G3*). The number of measurements is indicated above each genotype. Note that only the diameter of one distal lobe per gland was measured. Data represent ≥3 independent experiments. ***$p<0.0001$, one-way-ANOVA (Bonferroni's Multiple Comparison Test).

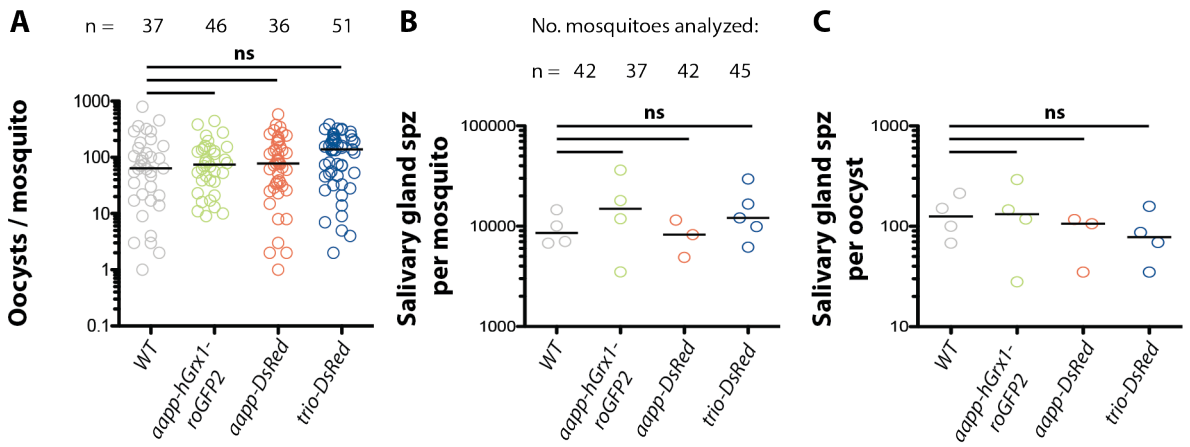

Figure 4. Oocyst densities and salivary gland colonization in *aapp-DsRed*, *aapp-hGrx1-roGFP2* and *trio-DsRed* mosquitoes infected with *P. berghei*.
Oocyst (**A**) and salivary gland sporozoite (spz) (**B**) counts in infected *aapp-DsRed*, *aapp-hGrx1-roGFP2* and *trio-DsRed* females in comparison to *wild type* (*G3*) females. Data pooled from three biological replicates. The total number of dissected mosquitoes is given above each genotype. **C)** Number of salivary gland sporozoites (spz) per oocyst for all three reporter lines in comparison to *wild type* (WT: *G3*). The invasion rate was calculated using the data shown in (A) and (B). Each dot represents a single mosquito (A) or the result of a counting (B and C), the median is indicated by a bar. All data were tested for significance using a one-way-ANOVA (Kruskal-Wallis test). ns: not significant (p>0.05).

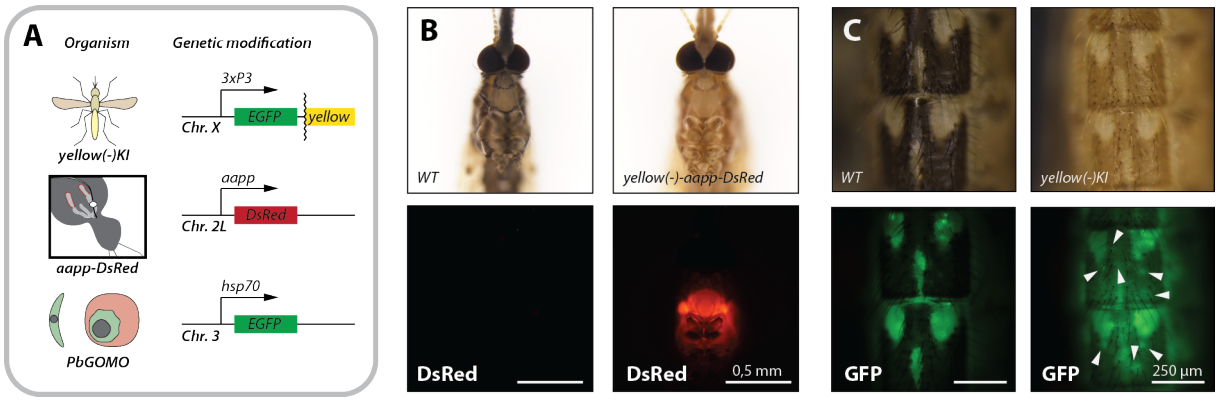

Figure 5. Salivary gland reporter lines as tool for *in vivo* imaging.
A) Genetic models used for *in vivo* imaging. Mosquitoes carrying the *aapp-DsRed* transgene were crossed with *yellow(-)KI* mosquitoes displaying reduced black pigmentation. Infections were carried out using the highly fluorescent *P. berghei* line *Δp230p-GFP* constitutively expressing EGFP (Manzoni *et al.*, 2015). **B)** Pigmentation phenotype and salivary gland-specific DsRed expression of *yellow(-)-aapp-DsRed* mosquitoes in comparison to wild type (WT: *Ngousso*). Brightfield and DsRed expression of the same field of view. Scale bar: 0.5 mm. **C**) Images of the abdomen of infected *yellow(-)KI* and wild type (*Ngousso*) mosquitoes. Brightfield and GFP expression of the same field of view. White arrows point towards oocysts visible through strong pigmented areas of the cuticle of *yellow(-)KI* mosquitoes. Scale bar: 250 µm.

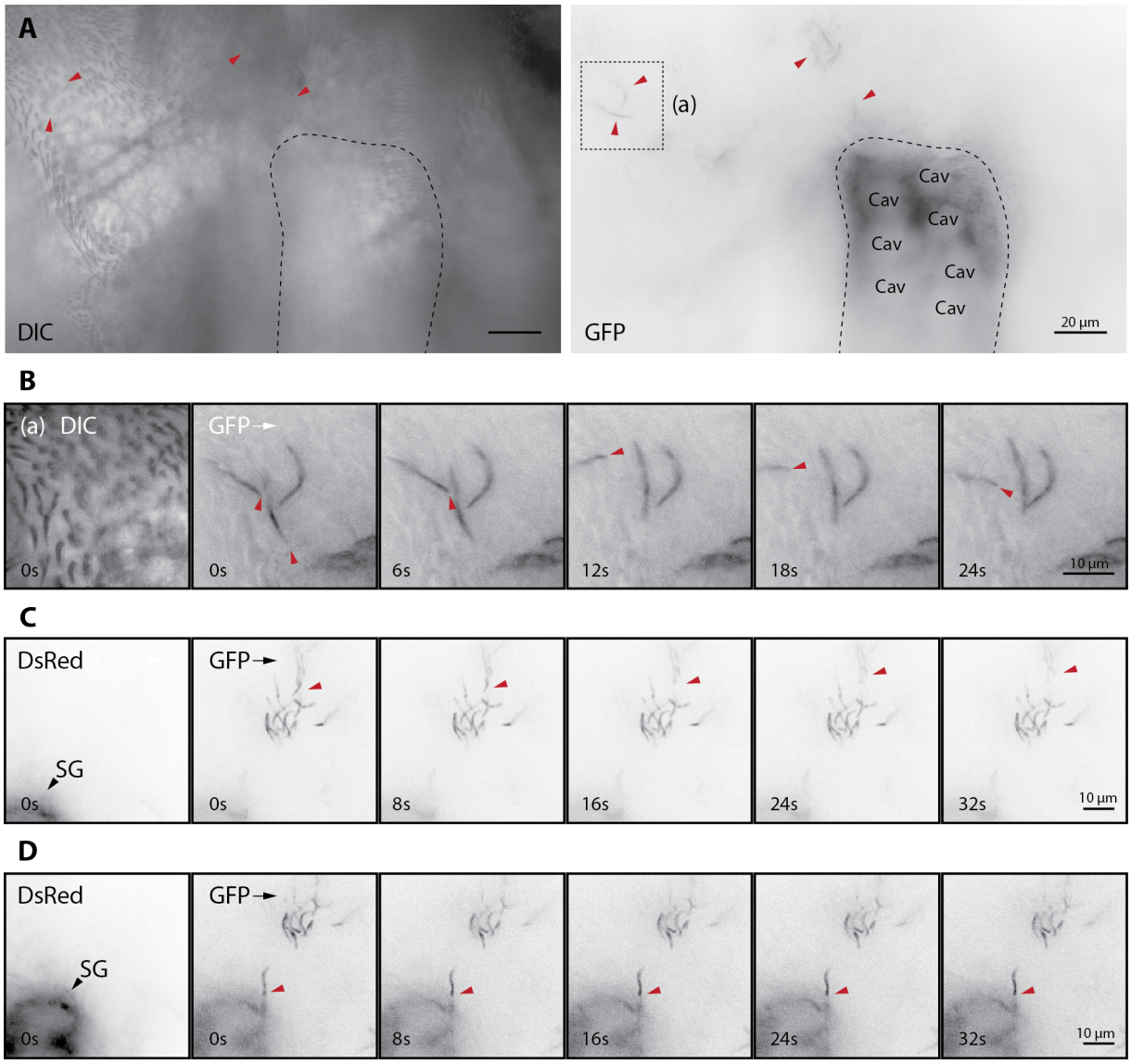

Figure 6. Confocal imaging of sporozoite salivary gland interactions in live mosquitoes. **A)** Thorax view of a *yellow(-)-aapp-DsRed* female mosquito infected with *P. berghei Δp230p-GFP*. Differential interference contrast (DIC) image on the left and the GFP signal on the right. Note that the DsRed expression in the salivary glands is strong enough to be visible in the GFP channel. Red arrows point towards sporozoites and the dashed line in the DIC image indicates the position of the salivary gland as seen in the GFP channel. Scale bar: 20 µm. **B)** Zoom on a group of sporozoites sequestered in close proximity to the salivary gland in the area boxed as (a) in the previous image (A). DIC image and a time series of the GFP signal with 6 s between frames. Red arrows point towards sporozoites displaying movement. Scale bar: 10 µm. **C,D)** Accumulation of sporozoites close to the salivary gland. **C** and **D** show the same salivary gland with altered focus and shifted field of view. DsRed signal (left) to indicate the position of the salivary gland (SG), and time series of the GFP signal with 8 s between frames. The red arrow points towards sporozoites displaying active movement (C) or towards a sporozoite in contact with the salivary gland (D). Scale bar: 10 µm. Note that imaging was performed with a Hamamatsu Orca Flash 4.0 V1 camera for A) and B) or a Yokogawa CSU X-1 for C) and D) using a 63-fold magnification objective (N.A. 1.4).

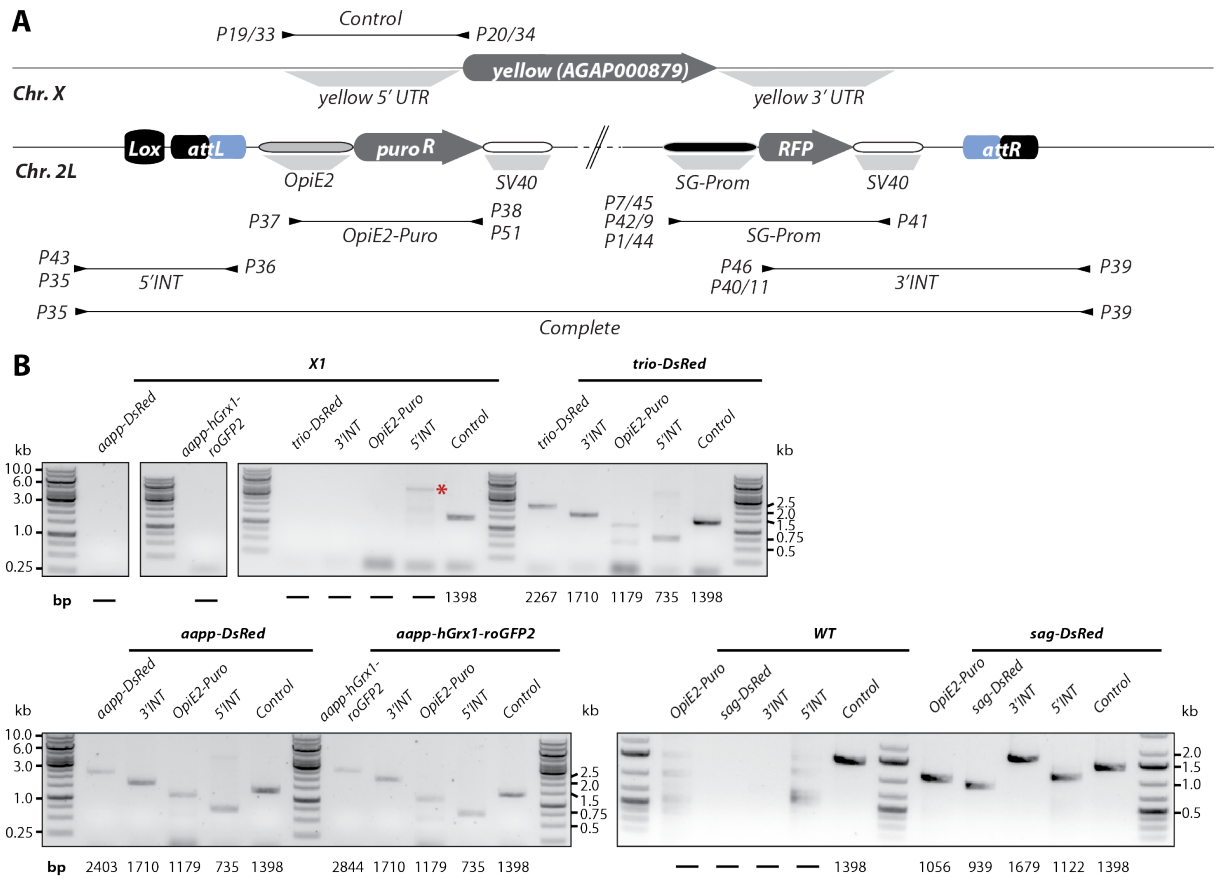

Figure S1. Genotyping of the salivary gland reporter lines *aapp-DsRed*, *aapp-hGrx1-roGFP2 and trio-DsRed*.

A) Schematic representation of salivary gland reporter transgenesis cassettes inserted on chromosome 2L. Fusion of *attB* and *attP* sites generate *attL* and *attR* sites after integration. The *Lox* site upstream of the transgene is a remnant of the fluorescence cassette initially required to select the docking line X1. Note that the illustration is not drawn to scale. **B)** Genotyping of generated transgenic mosquito colonies in comparison to *wild type* (WT: *G3*) or the parental line X1. Five different analytical PCRs were performed. The 5'INT and 3'INT PCRs amplify the integration borders upstream and downstream of the transgene, respectively. The presence of the puromycin resistance cassette was tested (OpiE2-Puro PCR). To ensure integration of the relevant fluorescence cassette, the PCRs aapp-DsRed, aapp-hGrx1-roGFP2, trio-DsRed and sag-DsRed were performed. In addition, a PCR control amplifying the 5'UTR of the *yellow* gene on chromosome X was included. Genotyping primers and amplified sequences are indicated with arrowheads and thin black lines in the scheme (A). The red asterisk marks an unspecific band only observed in the control X1.

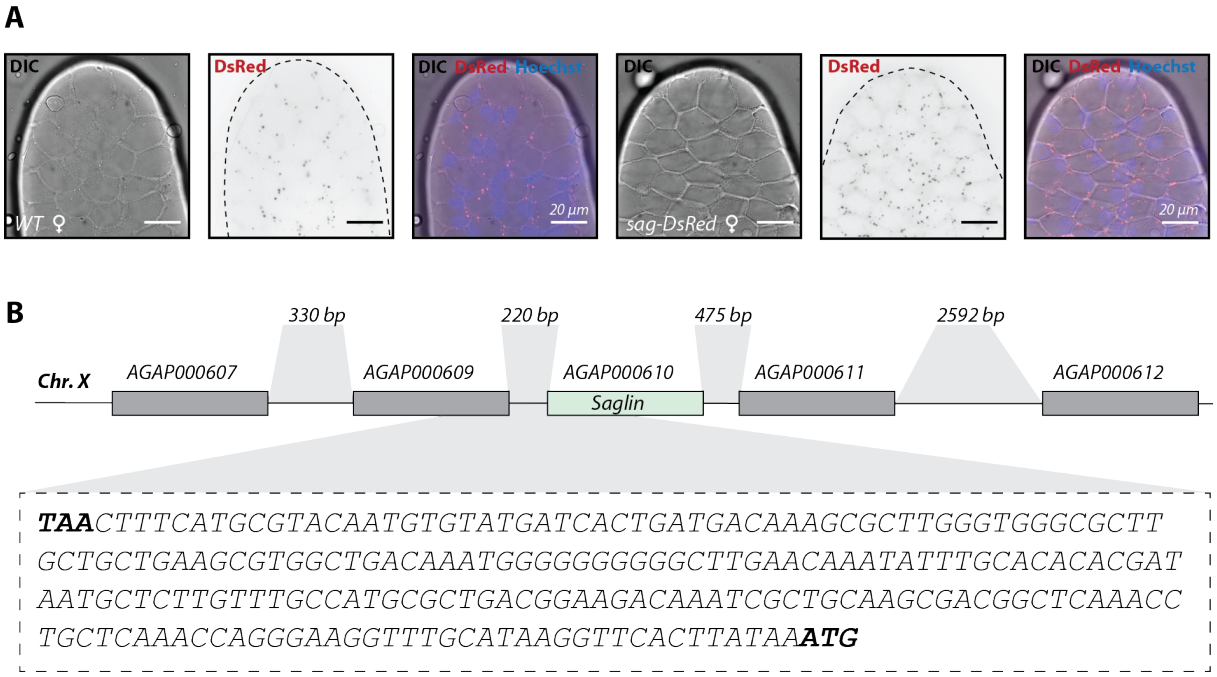

Figure S2. The intergenic sequence between AGAP000609 and AGAP000610 (*saglin*) displays no promoter activity.

A) Images of salivary glands from a *sag-DsRed* and a wild type female (*Ngousso*). Dissected glands were stained with Hoechst 33342 to detect the nuclei of acinar cells. The dotted black line in DsRed images indicates the outline of the salivary gland lobe observed in DIC. Scale bar: 20 µm. **B)** Genomic context of *saglin* (AGAP000610) with neighboring genes. The length of intergenic sequences is indicated above the scheme and the sequence tested for promoter activity located between AGAP000609 and *saglin* is shown. The stop codon TAA of AGAP000609 and the start codon of *saglin* are highlighted in black. The length of the cloned sequenced intergenic sequence was 220 bp (without stop codon of AGAP000609 and start codon of *saglin*). Note that the illustration is not drawn to scale.

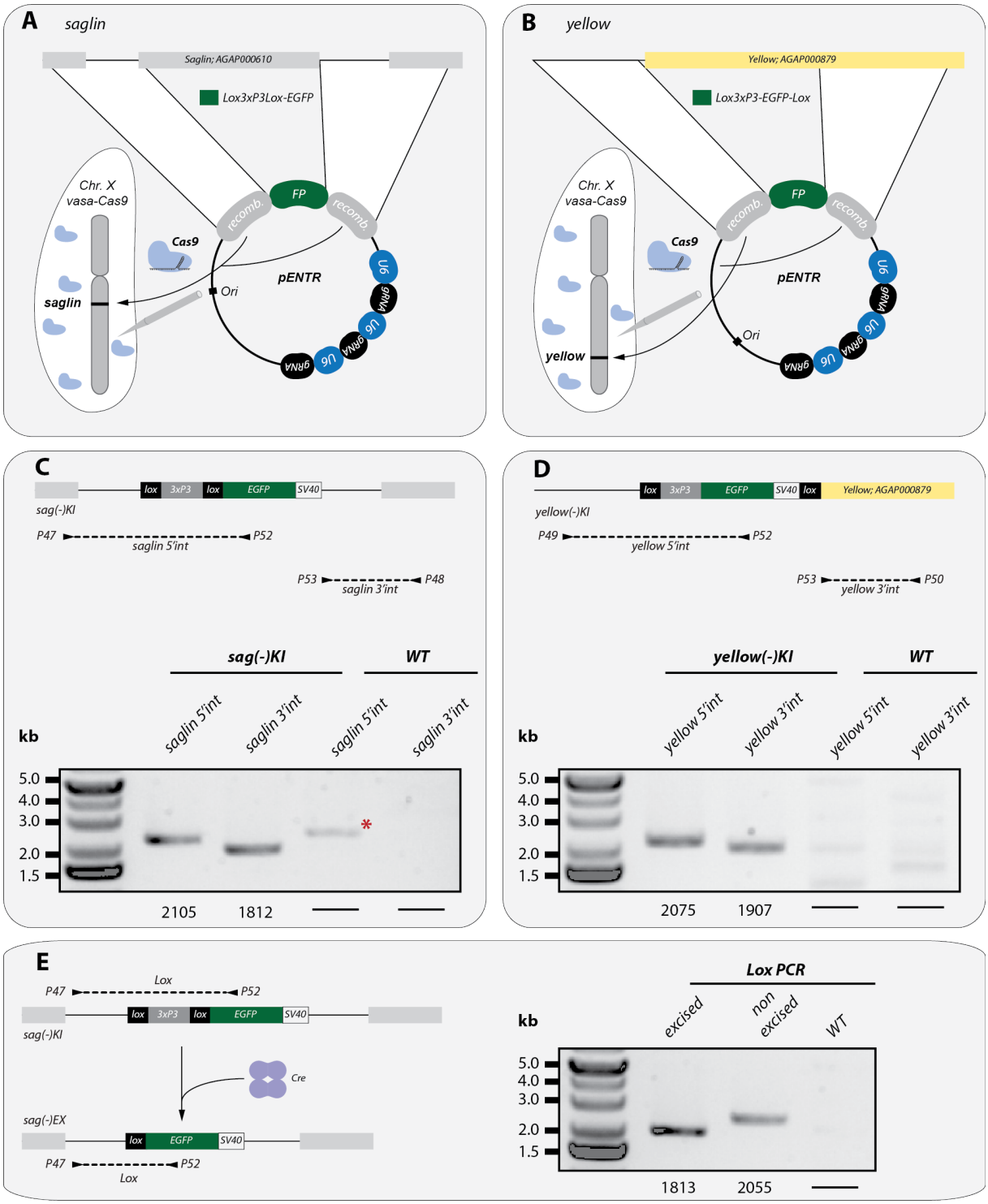

Figure S3. Genotyping of *sag(-)KI*, *sag(-)EX* and *yellow(-)KI* mosquitoes. *Sag(-)KI* (**A**) and *yellow(-)KI* (**B**) mosquitoes were generated by injecting embryos expressing Cas9 (*vasa-Cas9*) with plasmids carrying repair templates that contain a Lox3xP3Lox-EGFP or a Lox3xP3-EGFP-Lox cassette flanked with upstream and downstream sequences of the respective targeted locus, in combination with three guide RNAs specific for the *saglin* (AGAP000610) or *yellow* gene (AGAP000879). Genotyping of the 5' and 3' integration borders revealed successful integration of the transgenes into *saglin* (**C**) and *yellow* (**D**). The red asterisk marks an unspecific PCR product observed in the wild type control (WT: *Ngousso*). **E)** To investigate the native expression of the *saglin* promoter, the *3xP3* promoter

929 initially used to select transgenic *sag(-)KI* mosquito larvae was removed by Cre-mediated
930 excision. The loss of the *3xP3Lox* sequence in *sag(-)EX* mosquitoes was confirmed by PCR.
931

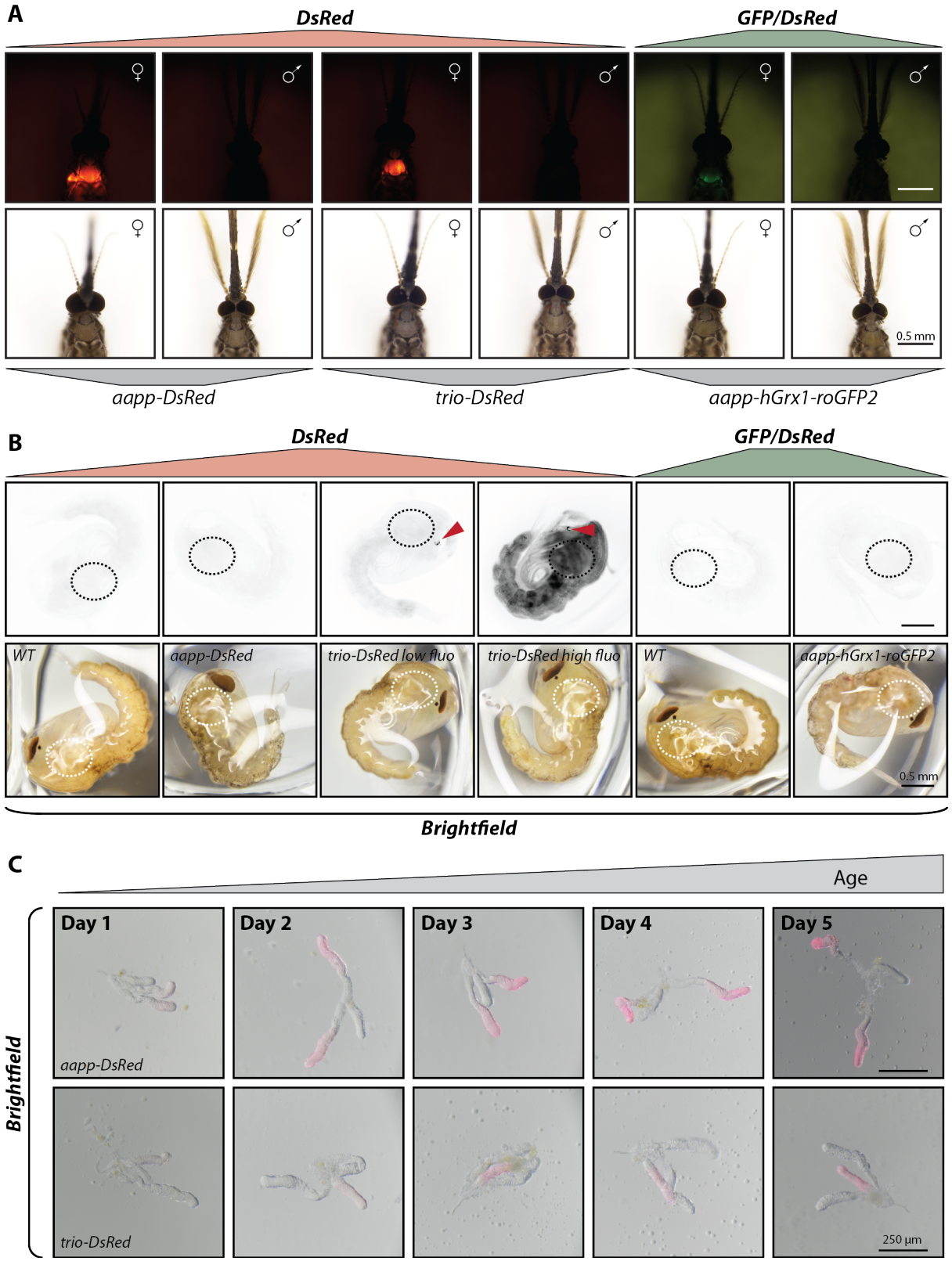

Figure S4. Expression driven by *trio* and *aapp* promoters is female- and adult-specific and the fluorescent reporter accumulates after the emergence of adults.
A) Fluorescence and brightfield images of female / male pairs of *trio-DsRed*, *aapp-DsRed* and *aapp-hGrx1-roGFP2* mosquitoes. Note that all depicted mosquitoes were bred in synchrony and were seven day old (+/- 1 day). Scale bar: 0.5 mm. **B)** Fluorescence and brightfield images of *aapp-DsRed*, *trio-DsRed* and *aapp-hGrx1-roGFP2* pupae in comparison

940 to *wild type* (*G3*). Dotted circles indicate the putative position of the salivary glands. *Trio-*
941 *DsRed* pupae with low and high DsRed body expression are shown for comparison. The red
942 arrows indicate DsRed positive ocelli observed in most *trio-DsRed* pupae. Scale bar: 0.5 mm.
943 **C)** Brightfield images of *aapp-DsRed* and *trio-DsRed* female salivary glands from day 1 to
944 day 5 after hatching (a single image per day and per line). All images were acquired using the
945 same settings. Scale bar: 250 µm.
946

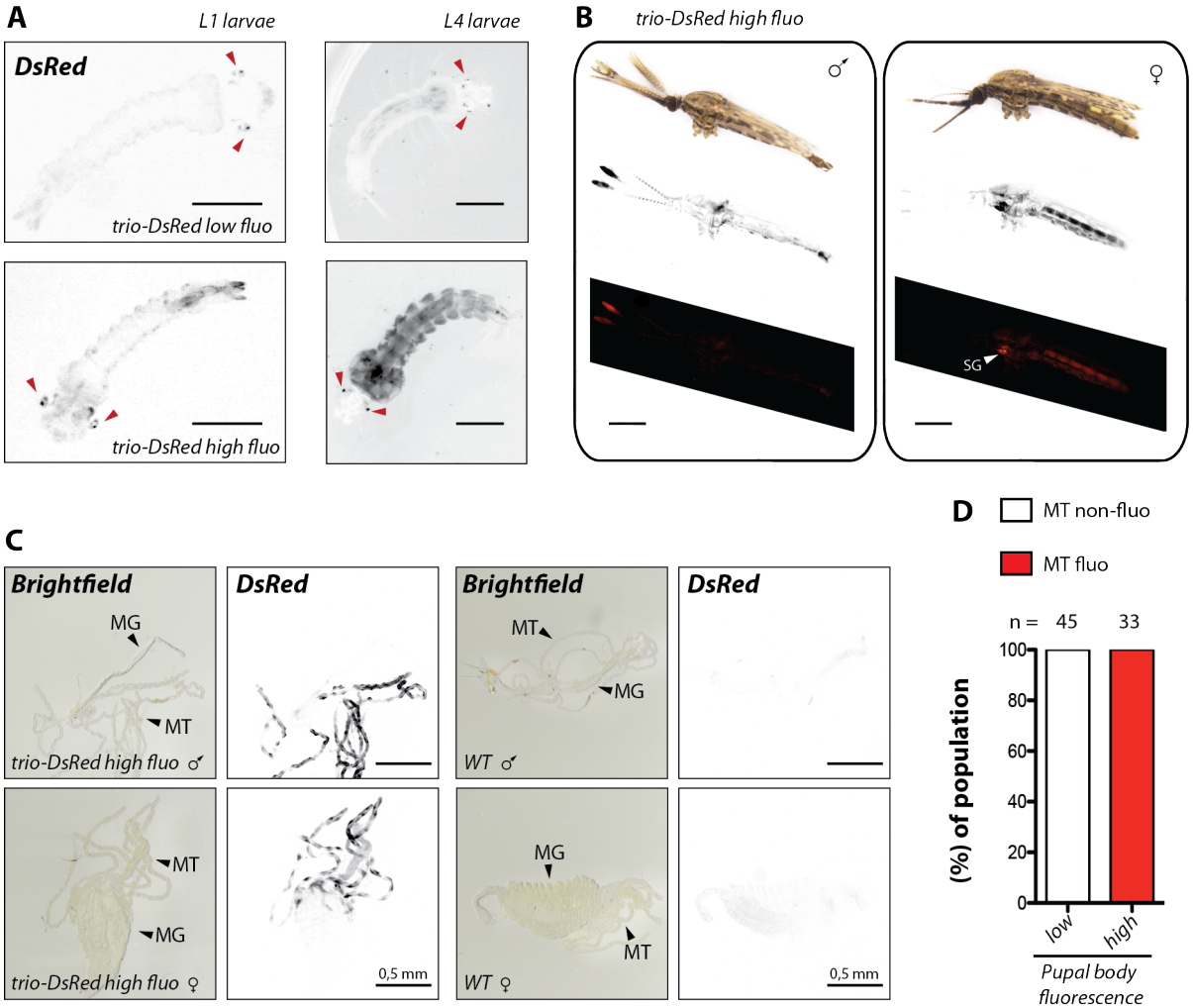

Figure S5. DsRed expression in Malphigian tubules (MT) of *trio-DsRed* mosquitoes is linked to ubiquitous DsRed expression in larvae, pupae and adults.
A) *Trio-DsRed* L1 and L4 larvae were classified as *trio-DsRed low fluo* or *trio-DsRed high fluo* according to their body DsRed fluorescence intensity. Red arrowheads point towards the DsRed positive eyes observed in the majority of larvae. Scale bar L1: 250 µm. Scale bar L4: 0.5 mm. **B)** Whole body fluorescence of *trio-DsRed high fluo* male and female mosquitoes. From top to bottom: brightfield, inverted DsRed fluorescence signal displayed in black and white and in red on black. Note that images were stitched from two separate images showing either the head or the abdominal part. Scale bar: 0.5 mm. **C)** Representative images of male and female midguts dissected from mosquitoes that displayed high body fluorescence at the pupal stage in comparison to *wild type* (WT: *G3*). Malphigian tubules (MT) and midguts (MG) are indicated by black arrows. Scale bar: 0.5 mm. **D)** Correlation of high body fluorescence at the pupal stage with DsRed expression in malphigian tubules (MT). Data were collected from two different mosquito generations. The number of analyzed mosquitoes is indicated above each column.

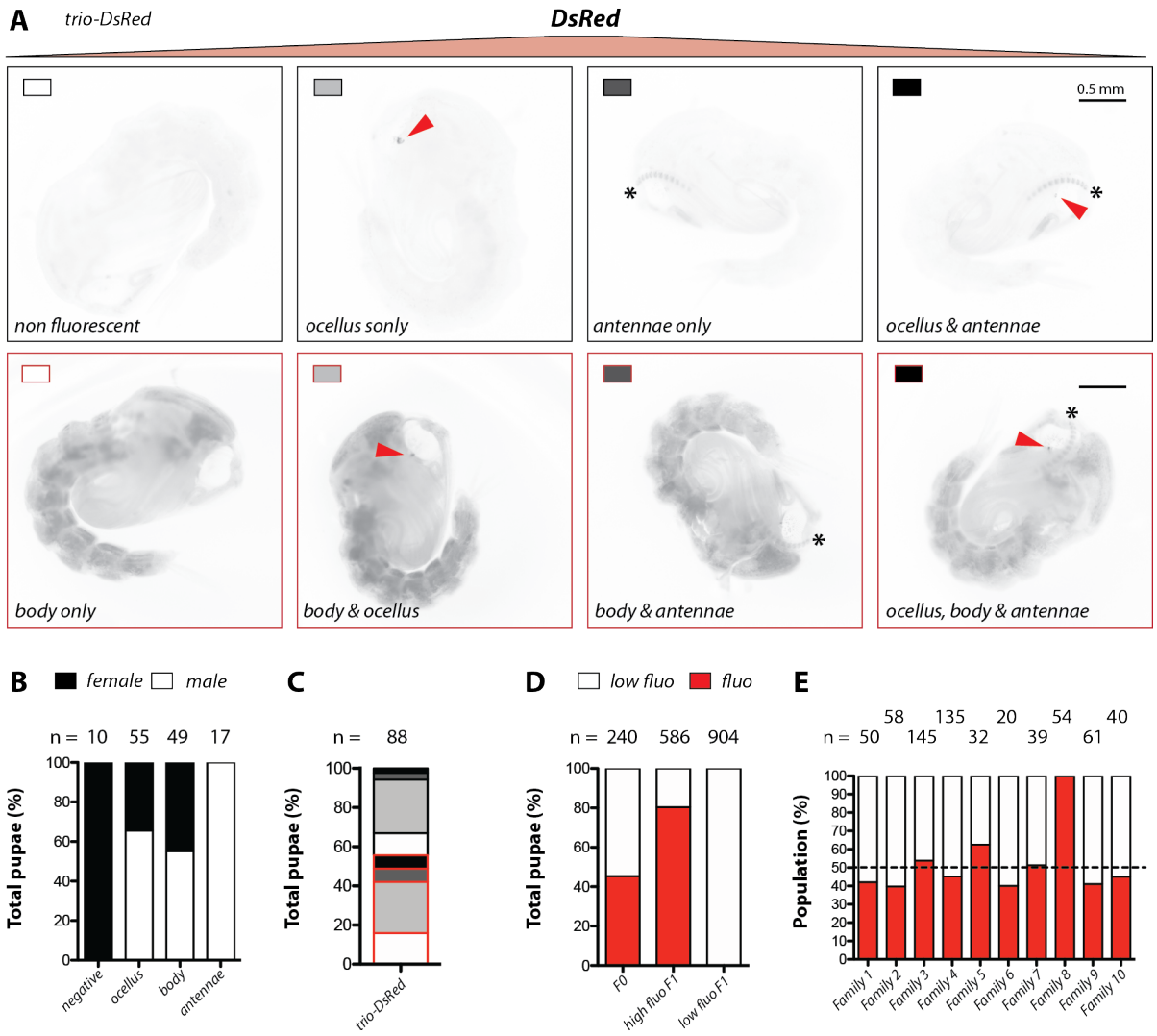

Figure S6. *trio-DsRed* pupae display high variability in DsRed expression.
A) Representative images of DsRed expression patterns in *trio-DsRed* pupae. A subpopulation of pupae displayed high body DsRed expression (images in red frames) while remaining pupae showed no DsRed body expression (black frames). Some pupae displayed fluorescent ocelli and/or fluorescent antennae. The presence of DsRed expression in body, ocelli and antennae occurred in different combinations that are represented by rectangles with different shades and frames. Scale bar: 0.5 mm **B)** Fluorescence patterns in pupae in relation to their sex. Non-fluorescent pupae were exclusively female while pupae with fluorescent antennae were exclusively male. Data pooled from four generations (≥20 pupae per generation). **C)** Proportion of each fluorescence pattern in relation to the whole population. Shading and framing of the different patterns as in (A). **D)** Proportion of pupae with high and low body fluorescence in the *trio-DsRed* colony (F0) and after intercrossing individuals displaying high or low pupal body fluorescence (F1). The number of analyzed individuals is given above each column. **E)** Females hatched from pupae with high body fluorescence analyzed in (D, high fluo F1) were kept separately and crossed to wild type males (*Ngousso*). The progeny of single females was evaluated at the pupal stage for body fluorescence (same color code as D, dashed line indicates 50% of the population). Females of families 5, 6, 7, 8 and 10 were also evaluated for salivary gland fluorescence which was present in all specimens.

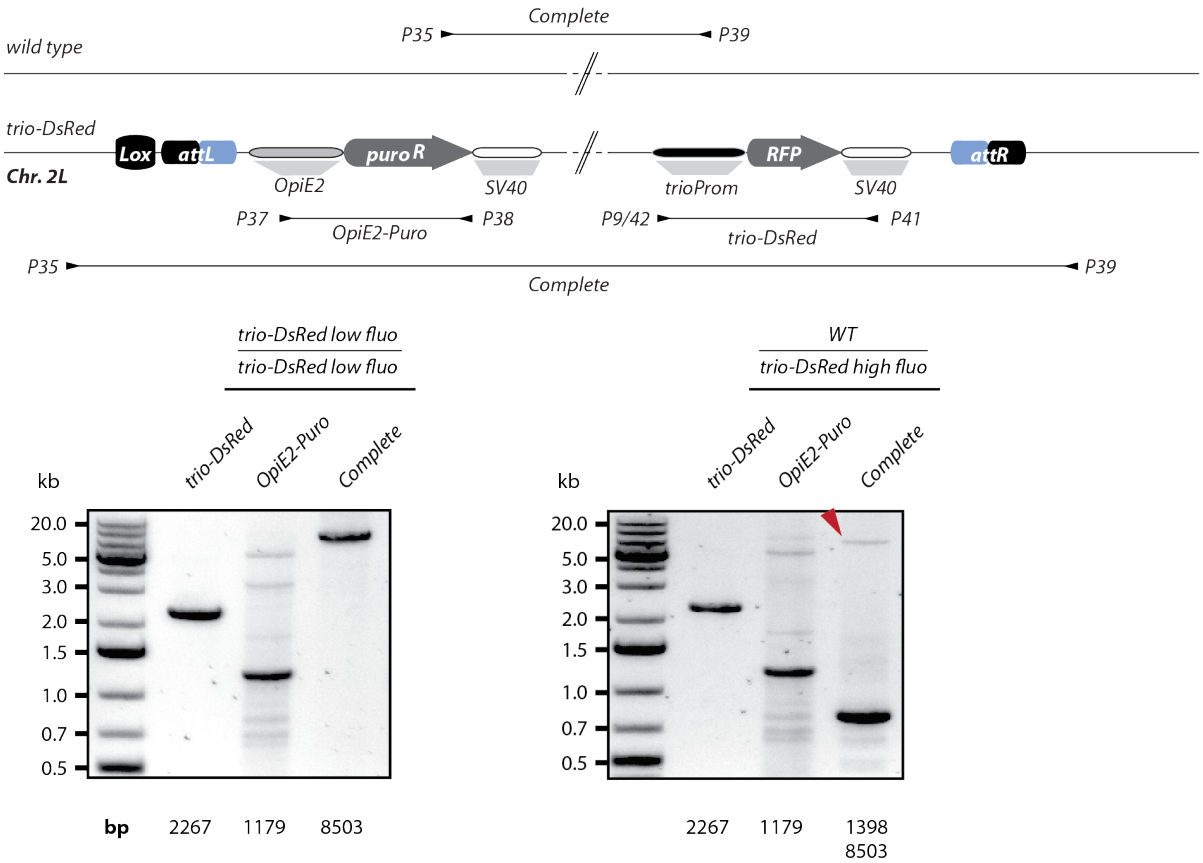

Figure S7. Genotyping of *trio-DsRed high fluo* in comparison to *trio-DsRed low fluo*. Genotyping of a female mosquito homozygous for the *trio-DsRed* low fluorescence transgene taken from the colony generated by crossing fluorescence negative pupae (see **Fig. S6D)** in comparison to a female mosquito heterozygous for the *trio-DsRed* high fluorescence transgene and the wild type allele obtained from family 1. An illustration of the modified X1 locus containing the *trio-DsRed* transgene in comparison to the unmodified wild type allele is shown on top. Genotyping primers and expected products are shown as black arrows and lines, respectively. The length of the expected PCR products is indicated below the gel images. Note that for the heterozygous female carrying the *trio-DsRed* high fluorescence transgene the smaller PCR fragment amplifying the unmodified locus dominates while the long PCR fragment representing the transgene containing allele is visible as a faint band at the upper edge (marked by a red arrow). The OpiE2-Puro PCR to verify the presence of the transgene gave several unspecific bands. PCRs were performed on genomic DNA obtained from single mosquitoes.

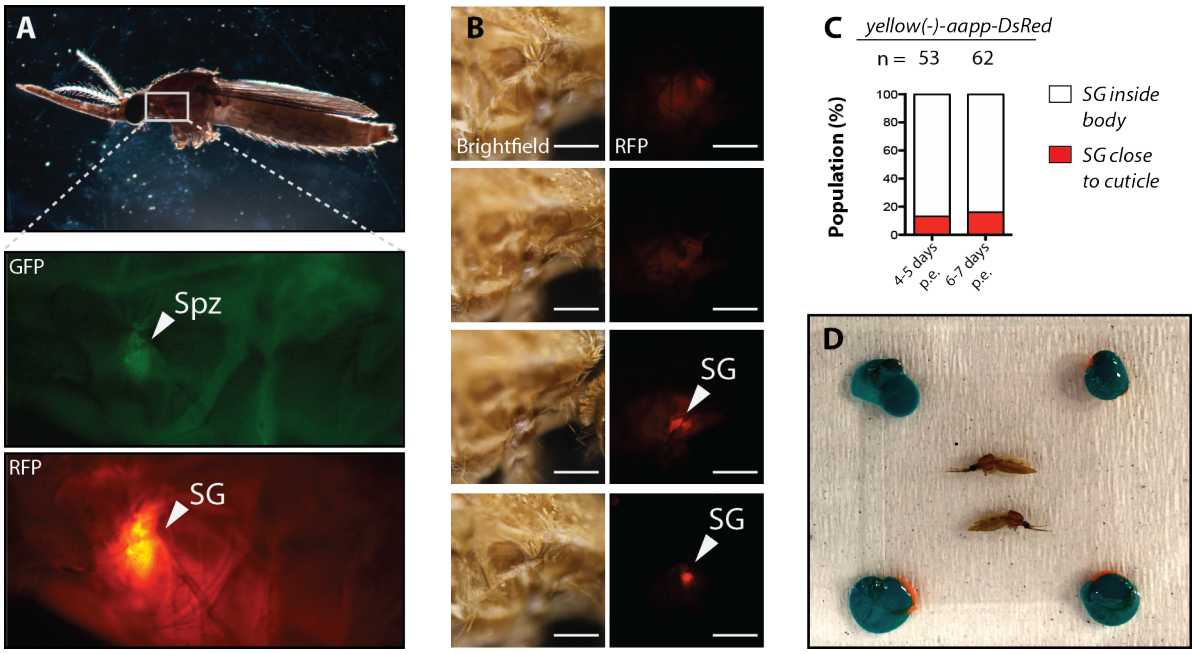

Figure S8. Selection and sample preparation of mosquitoes for *in vivo* imaging. **A)** Images of an infected mosquito with sporozoites (Spz, GFP channel) inside salivary glands and salivary gland (SG, red channel) localization close to the cuticle. GFP and DsRed images show the mosquito neck region squared in the brightfield image (top). **B)** Positioning of the salivary gland varies between mosquitoes, either deep (rows 1 & 2) or close to the cuticle (rows 3 & 4). Brightfield (left) and DsRed (right) images of the same field of view. Images were acquired with the same settings. Scale bar: 250 µm. **C)** Quantification of salivary gland positioning according to the fluorescence pattern shown in (B). Two mosquito batches were evaluated per time point post emergence (p.e.). The number of evaluated mosquitoes is indicated above each column. **D)** Sample preparation before imaging. Legless mosquitoes were glued on a microscopy slide and covered with a cover slip underlaid with orange plasticine to avoid squeezing. Corner areas were subsequently coated with teal-colored nail polish to prevent the cover slip from moving.

Movie 1. Sporozoites display active motility inside the mosquito.
Movie showing three sporozoites imaged in close proximity to the salivary gland. Sporozoites appear to be attached to a larger vessel and observed movements might be a mixture of active motility influenced by passive hemolymph flow. Imaging performed with a Hamamatsu Orca Flash 4.0 V1 camera using a 63x (NA 1.4) objective. GFP signal of a 3 min movie with 3 seconds between frames.

Movie 2. Sporozoites form accumulations close to the salivary gland.
Movie showing an accumulation of sporozoites close to the salivary gland directly below the cuticle. Several sporozoites display active back and forth movements. Imaging was performed with a Yokogawa CSU X-1 camera using a 63x (NA 1.4) objective. The left side of the movie displays the DsRed signal (salivary gland) while the right side shows the GFP signal (sporozoites) in black on white. Two min movie with 2 seconds between frames.

Movie 3. Sporozoite crawls through tissue by employing back and forth gliding.
Movie showing an actively moving sporozoite below the cuticle. The sporozoite was captured in proximity to the gland. By actively moving back and forth the sporozoite crawls slowly forward reaching eventually deeper tissues layers. Imaging was performed with a Yokogawa CSU X-1 camera using a 63x (NA 1.4) objective. The left side of the movie displays the DsRed signal (salivary gland) while the right side shows the GFP signal (sporozoites) in black on white. Two min movie with 2 seconds between frames.

Supplementary Table S1.

List of primers used for cloning plasmids to generate salivary gland reporter lines as well as *yellow(-)KI* and *sag(-)KI* lines. Nucleotides highlighted in green represent the cutting site for *Bsa*I. The guanin written in white on a black background indicates an undefined position of the *Bsa*I cutting site which can be any nucleotide. The nucleotides marked in red represent the overhangs needed for assembly of the GoldenGate building blocks. Sequences written in black define primer binding sites and nucleotides highlighted in orange represent overhangs to allow fusion of DNA sequences by assembly PCR.

Primer	Sequence (5' to 3')	Description
P1	GGTCTCGATCCCTTTTCTTTTACCCTTTGTAACACGCTAATAACG	aapp_5'UTR_forward
P2	GGTCTCGCTCTGTCGTTTTTTTGTTGTTGTGGTATTATTTCACTG	aapp_5'UTR_reverse
P3	GGTCTCGAGAGATGGCTCAAGAGTTTGTGAACTGCAAAATC	hGrx1-roGFP2_forward
P4	GGTCTCGAAGCTTACTTGTACAGCTCGTCCATGCCG	hGrx1-roGFP2_reverse
P5	GGTCTCGAGAGATGGTGCGCTCCTCCAAGAACG	DsRed_aapp/trio_forward
P6	GGTCTCGAAGCCTACAGGAACAGGTGGTGGCGGC	DsRed_aapp/trio_reverse
P7	GGTCTCGATCCTTTTCTGAGGTGATCTTTCGAAAAGATCG	trio_5'UTR_forward
P8	GGTCTCGCTCTGTAACTGGGAGCAGATTGATTTTATGG	trio_5'UTR_reverse
P9	GGTCTCGATCCCTTTCATGCGTACAATGTGTATGATCACTG	saglin_5'UTR_forward
P10	CGTTCTTGGAGGAGCGCACCATTTATAAGTGAACCTTATGCAAACCTTCCCTG	saglin_5'UTR_reverse

1071 1072	**P11**	CAGGGAAGGTTTGCATAAGGTTCACTTATA AATGGTGCGCTCCTCCAAGAACG	DsRed_saglin_forward
1073 1074	**P12**	GGTCTCGAAGCCTACAGGAACAGGTGGTGG CGG	DsRed_saglin_reverse
1075	**P13**	CCTTGTAGCGTGCCTGGTGGCCGC	Yellow_gRNA1_fw
1076	**P14**	AAACGCGGCCACCAGGCACGCTAC	Yellow_gRNA1_rev
1077	**P15**	CCTTGGCGACTACGTGCCCACGAA	Yellow_gRNA2_fw
1078	**P16**	AAACTTCGTGGGCACGTAGTCGCC	Yellow_gRNA2_rev
1079	**P17**	CCTTGGAGAACAAGCTGTTCGTCT	Yellow_gRNA3_fw
1080	**P18**	AAACAGACGAACAGCTTGTTCTCC	Yellow_gRNA3_rev
1081	**P19**	GGTCTCGAACAGAATTGAACGCCCAAGGTACGGCTG	Yellow_5’UTR_fw
1082	**P20**	GGTCTCACCCCGCTTCTGCCACTAAGGAACTTCTGTG	Yellow_5’UTR_rev
1083	**P21**	GGTCTCGAAGACGTGTGTCCTGGAAGTGTGATTTATCG	Yellow_3’UTR_fw
1084 1085	**P22**	GGTCTCGAAGCGTAGCGTGCCTGGTGGCCGCCGG AACGCTTTCCCTGCAGCGTAC	Yellow_3’UTR_rev
1086	**P23**	CCTTGCGTTCAAGTCATCTCGAGC	Saglin_gRNA1_fw
1087	**P24**	AAACGCTCGAGATGACTTGAACGC	Saglin_gRNA1_rev
1088	**P25**	CCTTGCCGCAGTCCTCGCGGCTGG	Saglin_gRNA2_fw
1089	**P26**	AAACCCAGCCGCGAGGACTGCGGC	Saglin_gRNA2_rev
1090	**P27**	CCTTGAAGTTTGCAACGTTTGCGA	Saglin_gRNA3_fw
1091	**P28**	AAACTCGCAAACGTTGCAAACTTC	Saglin_gRNA3_rev
1092	**P29**	GGTCTCGAACATGGGTTCACTCGCTGTTAGACTGTG	Saglin_5’UTR_fw

P30	GGTCTCAATGGTTATAAGTGAACCTTATGCAAACCTTCCCTG	Saglin_5'UTR_rev
P31	GGTCTCGAAGAGCGTCGGCGACGGTCTAAAAG	Saglin_3'UTR_fw
P32	GGTCTCGAAGCGTTCAAGTCATCTCGAGCCGG CTTCTTCTGCTGCCGCAGAAAC	Saglin_3'UTR_rev

1098 **Supplementary Table S2.**

1099 List of primers used for genotyping. Note that some primers used for construct cloning have
1100 also been used for analytical PCRs.
1101

Primer	Sequence (5' to 3')	Binding site
P33	GGTCTCGAACAGAATTGAACGCCCAAGGTACGGCTG	yellow_5'_forward
P34	GGTCTCACCCCGCTTCTGCCACTAAGGAACTTCTGTG	yellow_5'_reverse
P35	CCCGTCATGAGTTCAAGCCTGAA	X1_forward_1
P36	CCCGGTCTCAAATTGCCCGCCGTGACCGTCGA	attB_reverse
P37	CAAGCACCTTTATACTCGGTGGCCTC	OpiE2_forward
P38	TTCCAGGAAGGCGGGCACCCC	PuroR_reverse_1
P39	ACTGCAACCCATTCACACTG	X1_reverse
P40	CAGGGAAGGTTTGCATAAGGTTCACTTATAAATGGTGCGCTCCTCCAAGAACG	DsRed_forward
P41	CCTCTACAAATGTGGTATGGCTGA	SV40_reverse
P42	GGTCTCGATCCCTTTCATGCGTACAATGTGTATGATCACTG	sag_forward
P43	CCTTGAAGATTGGAATCCATCCAT	X1_forward_2
P44	GGTCTCGATCCCTTTTCTTTTACCCTTTGTAACACGCTAATAACG	aapp_forward
P45	GGTCTCGATCCTTTTCTGAGGTGATCTTTCGAAAAGATCG	trio_forward
P46	GGTCTCGAGAGATGGCTCAAGAGTTTGTGAACTGCAAAATC	hGrX1-roGFP2_forward
P47	GCTTATAAGAGCGCTACGGGTGTAC	Sag_5'_fw_genotyping
P48	CTGTCCCTTCAGCTTCACCAGCTC	Sag_3'_rev_genotyping
P49	GAACGACAGGTGAGCTGACAGTAAC	Yellow_5'_fw_genotyping

1128	**P50**	GATTTGGCGAGATGGTTTGTGCGAC	Yellow_3’_rev_genotyping
1129	**P51**	GAGCTCGAGTTCAGGCACCGGGCTTGC	PuroR_reverse_2
1130	**P52**	CTTCGGGCATGGCGGACTTG	EGFP_reverse
1131	**P53**	CAGCCATACCACATTTGTAGAG	SV40_forward

1132

Supplementary File S1.

Promoter sequences of the *trio*, *saglin* and *aapp* genes used to generate the mosquito lines *aapp-DsRed*, *aapp-hGrx1-roGFP2*, *sag-DsRed* and *trio-DsRed*. Nucleotides highlighted in red are part of the primer sequence used to amplify the promoter sequence. Sequences with a grey background indicate the 5'UTRs of the *trio* and *aapp* transcript, respectively.

***aapp* promoter sequence (AGAP009974, 1673 bp):**

CTTTTCTTTTACCCTTTGTAACACGCTAATAACGAAAGACCTCCTGCGTGTTAGTACG
TGGTGAGGATGATGCGTTTTAGCCTAGCTAGTATTCAAAAAACCTATTAATGCAACAATTAC
AGTGTGAGGTTACAAAATGGAATTAATTAAACACACTGCTCAACACAGCCATCGTGCTGCAT
CGTGCTTTGTTGAGGCGCAACAGTTAAATTGTAAGTGCAACCACCGGTATAGAGAGCTGCTT
TTGGCAAATGATATGGAATTGTGCTAAATTATGTAATGTTTTTTTTAACTAACTCGTTTACC
CGTTAATGGTGGAATGTTTGCAGGTGCGTAGATTAATTTTTTTTAAATGTGCAAATGGAGAA
AACAGGATAACGCAAAAGTATTTCCTTCGCTGTAGTAATAGGCTATTATTTATGTACGTCTT
TATGTGACCCCGCTAGTGTTGGCTGTATTTTATATCTGTAGGTAAATGACGCGCTATGTATT
GTAATAAAATTGGACAAACATTTGCATGTACGATCTGTTAGCTTAGAGAATAAGTATTTTTC
TTTTTCGCTACATTTCTCTAAATTCGACCGACGATGACTGTTTTAGGTGTTTTTTCGTAACT
TGATCAAGGTAACACCTTTTCTTGGCGTAACGTCCTACGCGGACATGCCGGCCGGCCTTATT
CAGGCTTTCGAGACTTAATTCATTACCACGTAGCCGGATAAGTCCAATCCTTGCACAACGGG
GGAACGGGTGTCCATTTCAGGCTTGGGCCCATGACGGGCATGTTATTGAGTCGTTCGAGTTG
ACGACTGTACCATGGGACCGCCCCATTTTTGGCAGTCCATTGATCGTTACGTCGTTTTACGT
CTACTGAAGGATGTCCGTTATCAGGTCAAGTCCAGCATAGATTAAGTCTCCCATACGAAGGA
TTGATTAGCTCGAGACTTAATGTTATATACAAAATTCTTATACATGTTCTAGATCAGGATTG
TTGCGCTACACTGTCTTCCATGTCGATCTTCTATATTCAGTTTTTGGCACAGTGATCGTCAC
TGTAATCTCAATAGATTTGAATTTCAATACTTCTATGGGAGGAGGATGAGTAGAAAGGTGTC
CAAAGCGCTGGATCTATGGCTGCAACTCCTCATGCTTGTAAGCACCCGACAGCCAATTCGAT
CTACCTGACCTGATGCGGTATTCGAACTAAAAGCACAGATCAAGCACTGTTTCACACGATCT
GAAGCACTGTTCTACTGCAAAGATAAGTGCATATTAGTTATTTTTCATACCGATCTTCACTG
CGACGGTTTAGCGATCTTCATTATTTTCCACCTTCACCCCTCAACCCAGGGAGTGCGCTTTT
CCCCGTCGAGATAAAATTACTAAATGTAAACTTTGCATGCAATTATGTAGCTGTATGGTAAG
CAAATAAAAATCTTTCCTCCTATTGCAACACGTCGCTTGTTTGCAGCGGATATTTGCCCACA
GTAAAGCCCGATCGCCTGTGCATTGTGTTTAACACGTGCTGCAAGCTGTATCAATACCGATC
GATTGTATGATTCCACGATCTTCGTGTGGTATAAAAACGGCGCTGAACAGCAGTAAAGATCA
TCACTTACATTTGTTTTATTCTCCACGGAGTCAGTGAAATAATACCACAACAACAAAAAAAC
G

***trio* promoter sequence (AGAP001374, 1537 bp):**

TTTTCTGAGGTGATCTTTCGAAAAGATCGATCGACCGACCCCCAACGGCAACTCTCCC
TCGGATGACCTCAGCCCAGAATAGGCATTCTTTCAGCAAGTCATTCTATCATCCCTTTTACA
TCTTACGTTACTCCAAAAAAAGAGAAGCTTTCCACCCCAAAGCTTTCGTTGTGGTGCAGCTT
TCGATGGTGATCGCGATCACGGTACCACACGTACGTTTGTTTGCTACTCTCGCTCACCGTTT
TCTTCGATTTCGTGTCTCGGGTACCGTTTGCTCGGTGCGGTAGTGCTGCGAAGAAAGCCGTT
GGCCGAGAGAATAATGCTCACTTCGGCTGCACGCAACTCGCCGTGCCACAGCCGTGGAAGGG
GTAGGTTGGATGGTCGGGGTCGGGACCGCAACGCCGAAGTGAACGCCGGCGTGCCAGCGAAC
GATCGCACCCCGGCACAGTCCAACTGCGTCGCTGGGCGCGCTCGGCGGACGGTTCTCGGTGT
GTGCGCCCCCTTTGGTGCTCATCCCTCATATCTCATCTCATCCTTTCGCGCTGCTCGCGGTT
CCCGCAGAACCACGCGCGAGAGGGAGTTGCGCGAACCAGGGAGAGCCCGACACCTGGGCAGC
GTCCAGGCGGACCTGTTCGGGAACGGTCGCGGTGTATAAAACTCGATTCCCGCCCGCCGTTA
GGTAACAGTCCATTGTGTAACGTTGCCGGGATCGCGAGCCATCCTGCAGGAACACAGCCGTG
CGAGTTTGTGTGCGCGTGTATTTTGCCTACAAGCAAGTGAGCAGCAATCAGTGAGAACAACA
TCTAAAACAGAAAAACAAACAGTGAACTACAGTGCTGTGGAGCAGTGGAAATTGGTGTTAAT
TGAAGAGCTTTGTACATCGATCACACGGACAACCACGCACGTGGAGAAAGTTCTGCTGCGGT
GCGGGTTACTTGCGTACACCACATTAAACATTGTGTGTGGCATTTAAAATAAATATACTCGC
GCCCTCCCCTCAGCTGCTCTCGCGGGCACGCCCGATGCCAGAGGTCGCCCCGACCGGACATT
GAACGTGGAAAGAAGAAAGTTGTCGGTTGTTTACACTTCCGTCCTGAGTGGTGTTGTGGCTA
CCGTTTGTGACCGTTGGTGAAATAAAGTAACATACCCCTCCCGAGGGCAGCAGCGACAATGA
CCTCCGGAAATTCGATAACAATACGTAAGTTACTTTCATTTTTTGCAAATTAAATTACCTCG
TGATAATTGAGTGGAGTGAGTAGGTACAGGTTGTTAACGCGTCTTTTGTTTAGTTCGGCAAT
CCGGATCCGAAGATGAGAGGAGATTGCCTCTGATGATGATGTTATCATGATTGCTTGTGTAA
CGACGCAAAGATTCTCAGAGAACAACTTCTCCCAACATAATTAATCTTGTTGAAGGGTCTGT
AAACACGTGGTGGGATATCTTACAACTGAACCAATATTCGACCGATAGTATAAAGTCCTTCG
CACCATCGATGCGTTTACCATTTTCCCATAAAATCAATCTGCTCCCAGTTACA

***sag* promoter sequence (AGAP000610, 220 bp):**

CTTTCATGCGTACAATGTGTATGATCACTGATGACAAAGCGCTTGGGTGGGCGCTTGC
TGCTGAAGCGTGGCTGACAAATGGGGGGGGGGGGGCTTGAACAAATATTTGCACACACGAT
AATGCTCTTGTTTGCCATGCGCTGACGGAAGACAAATCGCTGCAAGCGACGGCTCAAACCTG
CTCAAACCAGGGAAGGTTTGCATAAGGTTCACTTATAA